Gribisch, Bastian; Eckernkemper, Tobias

Intraday conditional value at risk: A periodic mixed-frequency generalized autoregressive score approach

Journal of Forecasting

Provided in Cooperation with:
John Wiley & Sons

Suggested Citation: Gribisch, Bastian; Eckernkemper, Tobias (2021) : Intraday conditional value at risk: A periodic mixed-frequency generalized autoregressive score approach, Journal of Forecasting, ISSN 1099-131X, Wiley, Hoboken, NJ, Vol. 40, Iss. 5, pp. 883-910, https://doi.org/10.1002/for.2744

Received: 19 June 2019 | Revised: 12 October 2020 | Accepted: 20 November 2020

DOI: 10.1002/for.2744

RESEARCH ARTICLE

WILEY

Intraday conditional value at risk: A periodic mixed-frequency generalized autoregressive score approach

Tobias Eckernkemper | **Bastian Gribisch**

Institute of Econometrics and Statistics, University of Cologne, Cologne, Germany

Correspondence
Bastian Gribisch, Institute of Econometrics and Statistics, University of Cologne, Universitätsstr. 22a, D-50937 Cologne, Germany.
Email: bastian.gribisch@statistik.uni-koeln.de

[Correction added on 3 March 2021, after first online publication: The order of authors in the author byline has been corrected.]

Abstract

We propose a copula-based periodic mixed frequency generalized autoregressive (GAS) framework in order to model and forecast the intraday exposure conditional value at risk (ECoVaR) for an intraday asset return and the corresponding market return. In particular, we analyze GAS models that account for long-memory-type of dependencies, periodicities, asymmetric nonlinear dependence structures, fat-tailed conditional return distributions, and intraday jump processes for asset returns. We apply our framework in order to analyze the ECoVaR forecasting performance for a large data set of intraday asset returns of the S&P500 index.

KEYWORDS

CoVaR, dynamic copulas, intraday, systemic risk

JEL CLASSIFICATION

C32; C51; C58G17

1 | INTRODUCTION

Intraday trading on financial markets has become increasingly important over the last decades and increased the need for traders and heads of trading desks to have within-day access to market information in order to make well-informed decisions. This finding spurred research on modeling the time-series characteristics of intraday returns, where recent contributions typically focus on univariate volatility modeling; see, for example, Engle and Sokalska (2012), Stroud and Johannes (2014), Rossi and Fantazzini (2015), and Bekierman and Gribisch (2017). Precise intraday volatility estimates are of considerable importance for intraday risk management, that is, analyzing and predicting intraday risk measures like the value at risk (VaR) as an ingredient for portfolio selection, hedging, and placing limit orders. As, for example, noted by Gourieroux and Jasiak (1997), intraday risk management is constantly used by commercial banks in order to monitor their internal trading desks. For example, traders have to be able to constantly provide estimates of their risks during the trading day. Although daily risk measures may be adequate from a reporting perspective, traders typically need up-to-date information on their risks in order to have competitive advantages by reacting on risks in real time (see also Liu & Tse, 2015).

In addition to the pure volatility aspect, financial risk management increasingly focusses on the assessment of dependencies in the tails of the bivariate return distribution of the asset and the market: while the popular VaR measure focusses on the single institution, more up-to-date approaches incorporate systemic tail risk effects via the connection of the institution with the whole financial system. Prominent examples are the exposure conditional VaR (ECoVaR) and the ΔECoVaR of Adrian and Brunnermeier (2016). These measures are important ingredients for the assessment of spillover and contagion effects and the connectedness in network analysis and

allow to reveal those institutions that are most at risk if a financial crisis occurs (see, e.g., Bernardi & Catania, 2016; Chen et al., 2019; Girardi & Ergün, 2013; Reboredo & Ugolini, 2015). According risk estimates are clearly of interest from an intraday monitoring perspective, where the single trader is, for example, asked to provide an estimate of the within-day vulnerability of his portfolio to systemic effects.

While aspects of intraday VaR modeling have already been discussed in the literature, we are not aware of contributions on the intraday modeling of systemic risk measures. In fact, approaches based on daily data may easily oversee important risk spillovers within the trading day, as, for example, a zero open to close return on a given trading day might still be the result of heavy return variation within the day with eventually hidden systemic effects for the market as a whole. Derived intraday asset linkages within the tails of the distribution might also be of interest for high-frequency contagion and network analysis, which become more and more important since crisis often reveal patterns of high-speed information transmission through markets.

In this paper, we propose a mixed frequency generalized autoregressive score (MF-GAS) framework (see Creal et al., 2013) in order to model and forecast the intraday (Δ)ECoVaR measure. The (Δ)ECoVaR captures tail-specific risk spillovers for the bivariate relationship of an intraday asset return and the market by providing information on the VaR of the individual asset conditional on the market being in distress. The computation of this systemic risk measure requires a bivariate modeling of the intraday asset and market return while accounting for long-memory type of dependence patterns in the volatility and dependence processes, seasonalities, and potential asymmetries in tail dependence. In particular, we propose to model the bivariate asset–market relationship in a dynamic seasonal copula framework with time-varying volatilities and (a)symmetric tail dependencies. Based on the copula specification, we obtain forecasts of the (Δ)ECoVaR in a straightforward way by using the approach of Mainik and Schaanning (2014) and Reboredo and Ugolini (2015).

The copula approach allows us to separate the joint distribution into the dependence process and the margins. The modeling of the marginal distribution of intraday asset returns is challenging for several reasons: the returns feature heavy tails, discrete jump components, and long-memory type of persistencies and periodicity in the volatility process. Standard generalized autoregressive conditional heteroskedasticity (GARCH) models (Bollerslev, 1986; Engle, 1982) have therefore proven to be unsatisfactory for intraday return dynamics (see, e.g., Andersen & Bollerslev, 1997). A popular approach to intraday volatility modeling is to factorize the conditional variance into a product of daily and intraday components (see, e.g., Andersen & Bollerslev, 1997, 1998), where the daily component captures the long-range dependence in the volatility series. Engle and Sokalska (2012) use commercially available volatility forecasts in order to approximate the daily volatility part. The remaining intraday fluctuations are then modeled by short-memory GARCH processes, where periodic intraday volatility patterns can be estimated individually or approximated by flexible Fourier forms (see, e.g., Payne, 1996).[1] An alternative approach, which has, for example, been analyzed by Rossi and Fantazzini (2015), builds on periodic fractional integrated exponential GARCH (FI-PEGARCH) models for the intraday return series. A similar (though nonperiodic) approach has been used by Janus et al. (2014) in order to model long-memory dynamics in the copula dependence parameters for daily asset returns. A fractionally integrated GAS (FIGAS) approach for daily returns is analyzed by Opschoor and Lucas (2019). ARFIMA-type processes model 'true' long memory but tend to induce complications and instability in model estimation and suffer from problems related to the initialization of the long-memory process.

Our approach in contrast builds on mixed frequency GAS dynamics for the individual asset log-volatilities and the dynamic copula parameters. The mixed frequency structure offers a flexible and robust approximation to long-memory while preserving stationarity of the volatility and dependence components and computational ease of estimation. The model builds on latent short-term and long-term components that move at different frequencies. Here, we assume that the long-term component moves at the daily and the short-term component at the intraday frequency, which results in a framework that is similar in spirit to the Engle and Sokalska (2012) approach but explicitly models the long-term component instead of using exogenously determined commercial forecasts. The model also shows similarities to the popular mixed data sampling (MIDAS) schemes for volatility modeling (see, e.g., Colacito et al., 2011; Engle et al., 2013; Ghysels et al., 2006) but is more close to the stochastic volatility (SV) literature due do the flexible GAS assumption (see, e.g., Koopman et al., 2016).

Although not formally belonging to the class of long-memory models, multiple component models are well known to reproduce highly persistent long-memory type of dependence structures by aggregating independent autoregressive dynamics at different frequencies (see,

[1]Related studies on the component-modeling of intraday volatilities are found in Andersen and Bollerslev (1997, 1998), Bekierman and Gribisch (2017), and Beltratti and Morana (1999).

e.g., Corsi, 2009; Granger, 1980; LeBaron, 2001). A further advantage of using latent volatility components is that the dynamic mixed frequency GAS structure can easily be applied in order to model the dynamics of the copula dependence parameter, where, for example, MIDAS schemes or the Engle and Sokalska model are not directly applicable. The GAS approach optimally approximates the innovation terms of the latent state processes by scaled likelihood scores, which makes the model very flexible but still simple to implement.[2] The framework has also the advantage that the optimal frequency for the long-term component can be selected fully data-driven by comparing the log-likelihood values obtained for different frequencies and choosing the frequency associated with the highest log-likelihood value. We finally extend our basic model specification by considering conditional fat-tailed distributions and GAS-driven autoregressive Poisson jump processes for the marginal return specifications. For the copula models, we consider the Gaussian copula, the Student t copula and a mixture of the Clayton and the rotated Clayton copula in order to allow for (a)symmetric and possibly periodic tail dependence.

In fact, the application of GAS models with mixed frequencies is not new to the literature. Gorgi et al. (2019) propose a MIDAS-GAS model for economic time series like inflation or GDP growth, where a low-frequency economic variable is to be forecasted based on high-frequency financial information using a weighted sum of the high-frequency GAS innovations. This setting differs from our MF-GAS approach and the high-frequency financial data perspective: the MIDAS-GAS of Gorgi et al. (2019) models mixed frequency data using latent GAS-driven components at the lower frequency, while the MF-GAS considers low- and high-frequency GAS components in order to model data, which is observed at a single frequency. Our intraday copula approach also shows some similarities to recent work of Koopman et al. (2018). The authors propose a GAS driven copula framework for U.S. financial stocks at the tick-by-tick frequency and are particularly interested in analyzing the intraday dependence structure. In contrast to our approach, the model of Koopman et al. (2018) does not allow for long-memory type of dependence patterns and does neither consider periodicity in the tail-dependence nor model the intraday periodicity jointly with the GAS dynamics (which turns out to be crucial for intraday (Δ)ECoVaR forecasting; see below). The model is furthermore fitted separately for each trading day, which stands in contrast to our mixed-frequency approach for intraday volatility/dependence across trading days.

We provide an empirical application to a data set of the 378 most liquid stocks from the S&P500, which have been jointly traded between 2004 and 2012. We focus on analyzing the mixed frequency structure, long memory-type of dependencies and seasonalities in intraday variances, correlations, tail-dependencies, and jumps as well as their effects on the resulting (Δ)ECoVaR estimates. We find strong evidence of long memory and seasonalities in the intraday variance and dependence processes. Residual diagnostics show that the proposed mixed frequency GAS model successfully captures these effects. Furthermore, we find that those model specifications that allow for fat-tailed conditional return distributions and symmetric intraday tail dependencies are preferred. We also perform an in-sample and out-of-sample analysis in order to analyze (i) the time series behavior of the intraday (Δ)ECoVaR and (ii) the effect of seasonalities in the volatility and dependence processes on the (Δ)ECoVaR forecasts. Our results show significant intraday variation and periodicity of the (Δ)ECoVaR and that the modeling of seasonalities in the volatility and dependence process is essential in order to obtain reliable (Δ)ECoVaR forecasts.

The remainder of the paper is organized as follows. Section 2 gives an overview on the ECoVaR measure. Section 3 presents the mixed-frequency GAS model for intraday volatility and dependence including the model extension to price jumps. The application of the mixed-frequency GAS model to a large dataset of intraday asset returns of the S&P500 index is provided in Section 4. Finally, Section 5 summarizes the results and concludes.

2 | (Δ)ECoVaR

The CoVaR of the market (or the financial system) conditional on institution i is defined as the VaR of the market return conditional on the event that institution i is in distress (see Adrian & Brunnermeier, 2016; Girardi & Ergün, 2013).[3]

Let $r_{i,\tau}$ denote the return of institution i in period τ and $r_{m,\tau}$ the corresponding return of the market. The CoVaR is then the β-quantile of the conditional distribution of $r_{m,\tau}$:

$$Pr\left(r_{m,\tau} \leq CoVaR^{m|i}_{\alpha,\beta,\tau} \mid r_{i,\tau} \leq VaR^{i}_{\alpha,\tau}, \mathcal{F}_{\tau-1}\right) = \beta. \quad (1)$$

[2]GAS dynamics (Creal et al., 2013) have been intensively used in recent years in order to approximate the dynamics of unobserved component models. Theoretical justifications for the use of the conditional score as a flexible updating mechanism are, e.g., provided by Harvey (2013), Creal et al. (2013), and Blasques et al. (2015). Applications of score driven dynamics are, e.g., found in Creal et al. (2011), Janus et al. (2014), Harvey and Sucarrat (2014), and Eckernkemper (2018).

[3]Here and in the following sections, we will for simplicity refer to a single institution i. We however note that for risk management applications, the single institution is typically replaced by a portfolio of institutions.

The VaR for institution i, $VaR^i_{\alpha,\tau}$, is defined as the α-quantile of the conditional return distribution of asset i in period τ, $Pr(r_{i,\tau} \leq VaR^i_{\alpha,\tau})|\mathcal{F}_{\tau-1}) = \alpha$, where $\mathcal{F}_\tau$ denotes a filtration of the returns of the asset and the market up to period τ.

In order to measure the part of the systemic risk, which is caused by the distress of institution i, we may compute the ΔCoVaR as defined by Adrian and Brunnermeier (2016) and Girardi and Ergün (2013):

$$\Delta CoVaR^{m|i}_{\alpha,\beta,\tau} = \frac{CoVaR^{m|i}_{\alpha,\beta,\tau} - CoVaR^{m|\text{bench}^i}_{\beta,\tau}}{CoVaR^{m|\text{bench}^i}_{\beta,\tau}}, \quad (2)$$

that is, the additional effect on the VaR of the market if institution i is in distress, relative to the situation, where the return of institution i is at its benchmark level. Here, the benchmark level is defined as one standard deviation about the mean event, conditional on $\mathcal{F}_{\tau-1}$:

$$Pr\Big(r_{m,\tau} \leq CoVaR^{m|\text{bench}^i}_{\beta,\tau} \mid \mu_{i,t} - \sigma_{i,t} \leq r_{i,\tau} \leq \mu_{i,t} + \sigma_{i,t}, \mathcal{F}_{\tau-1}\Big) = \beta, \quad (3)$$

where $\mu_{i,t}$ and $\sigma_{i,t}$ denote the mean and standard deviation of the conditional distribution of $r_{i,\tau}$ given $\mathcal{F}_{\tau-1}$. The ΔCoVaR measures the systemic risk part which comoves with the distress of institution i and can therefore be interpreted as a statistical tail dependence measure (see Adrian & Brunnermeier, 2016). While the CoVaR itself is highly dependent on the conditional variance of the market return, the ΔCoVaR is mainly driven by the covariance between the market and the institution.

The (Δ)CoVaR as defined above is typically used in order to measure systemic risk contributions. In this paper, however, we are particularly interested in the risk management perspective. Here, it appears useful to reverse the conditioning of the CoVaR in order to obtain the exposure CoVaR (labeled ECoVaR) as proposed by Adrian and Brunnermeier (2016):

$$Pr\Big(r_{i,\tau} \leq ECoVaR^{i|m}_{\alpha,\beta,\tau} \mid r_{m,\tau} \leq VaR^m_{\alpha,\tau}, \mathcal{F}_{\tau-1}\Big) = \beta, \quad (4)$$

where $VaR^m_{\alpha,\tau}$ denotes the VaR of the market. According to Equation (2), the ΔECoVaR is then defined as

$$\Delta ECoVaR^{i|m}_{\alpha,\beta,\tau} = \frac{ECoVaR^{i|m}_{\alpha,\beta,\tau} - ECoVaR^{i|\text{bench}^m}_{\beta,\tau}}{ECoVaR^{i|\text{bench}^m}_{\beta,\tau}} \quad (5)$$

and measures the institution's (or the portfolio's) exposure to system-wide distress relative to a normal market situation. In the remainder of the paper, we will focus on the (Δ)ECoVaR.

3 | MF-GAS MODELING OF INTRADAY (Δ)ECOVAR

The computation and forecasting of the ECoVaR requires a joint conditional distribution for the asset- and market return. A flexible way of modeling this distribution is provided by the copula approach, where the joint conditional distribution is decomposed into the marginal distributions and the dependence structure, which is captured by a copula function (see, e.g., Nelsen, 2006, for an introduction to copulas). An attractive feature of the copula approach is that it allows to compute the ECoVaR in a straight-forward way (see Mainik & Schaanning, 2014; Reboredo & Ugolini, 2015). In particular, we can rewrite Equation (4) as

$$\frac{Pr\left(r_{i,\tau} \leq ECoVaR^{i|m}_{\alpha,\beta,\tau}, r_{m,\tau} \leq VaR^m_{\alpha,\tau} \mid \mathcal{F}_{\tau-1}\right)}{Pr\left(r_{m,\tau} \leq VaR^m_{\alpha,\tau} \mid \mathcal{F}_{\tau-1}\right)} = \beta, \quad (6)$$

resulting in

$$Pr\Big(r_{i,\tau} \leq ECoVaR^{i|m}_{\alpha,\beta,\tau}, r_{m,\tau} \leq VaR^m_{\alpha,\tau} \mid \mathcal{F}_{\tau-1}\Big) = F_{r_{i,\tau},r_{m,\tau}}\Big(ECoVaR^{i|m}_{\alpha,\beta,\tau}, VaR^m_{\alpha,\tau}|\mathcal{F}_{\tau-1}\Big) = \alpha\beta, \quad (7)$$

where $F_{r_{m,\tau},r_{i,\tau}}$ denotes the joint cumulative distribution function of $r_{i,\tau}$ and $r_{m,\tau}$ given all lagged return information. Following the Sklar (1959) theorem, we now express the joint cumulative distribution function by a conditional copula function,

$$C(u_{i,\tau}, u_{m,\tau}|\mathcal{F}_{\tau-1}) = \alpha\beta, \quad (8)$$

with $u_{i,\tau} = F_{r_{i,\tau}}(ECoVaR^{i|m}_{\alpha,\beta,\tau}|\mathcal{F}_{\tau-1})$ and $u_{m,\tau} = F_{r_{m,\tau}}(VaR^m_{\alpha,\tau}|\mathcal{F}_{\tau-1}) = \alpha$. Given known (or estimated) marginal distribution functions and copula the ECoVaR can be computed via a two-step procedure:

1. Solve $C(u_{i,\tau}, \alpha|\mathcal{F}_{\tau-1}) = \alpha\beta$ for $u_{i,\tau}$;
2. Compute $ECoVaR^{i|m}_{\alpha,\beta,\tau}$ via $ECoVaR^{i|m}_{\alpha,\beta,\tau} = F^{-1}_{r_{i,\tau}}(u_{i,\tau}|\mathcal{F}_{\tau-1})$.

For the computation and forecasting of the ECoVaR, we employ parametric specifications for the conditional return distributions and the bivariate copula function. In the upcoming two sections, we therefore develop flexible dynamic volatility models for intraday asset returns and dynamic copula specifications, which account for the time-varying and potentially nonlinear dependence between the intraday asset and market return.

3.1 | Volatility

3.1.1 | The V-MF-GAS Model

Let $P_{t,\ell}$ denote the intraday price of a particular asset at day t, $t = 1, \ldots, T$, and intraday period ℓ, $\ell = 1, \ldots, S$, where S is the total number of intraday periods per trading day (e.g., $S = 390$ for minute-returns). For the ease of notation, we define the overall period index $\tau = (t-1)S + \ell$

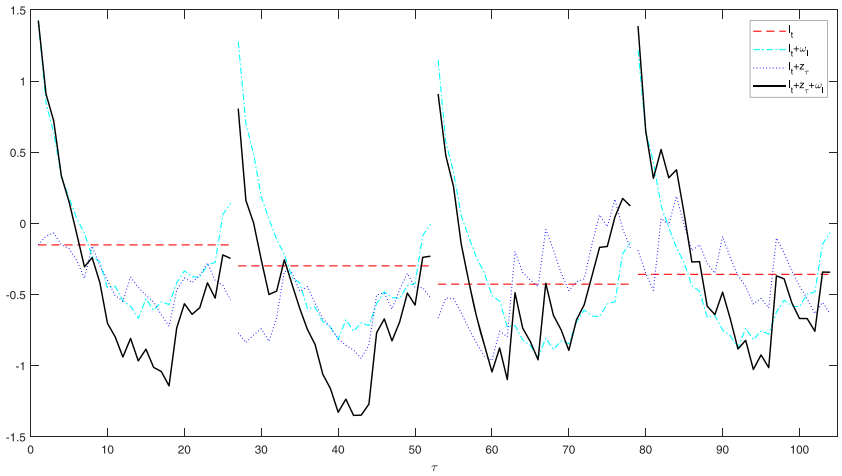

FIGURE 1 Total volatility and its components. Total log-volatility (solid black), intraday (dashed dark blue), and diurnal (dotted light blue) volatility components fluctuating around the daily (dashed red) volatility level for $S = 26$ intraday periods (corresponding to 15-min returns) and four trading days [Colour figure can be viewed at wileyonlinelibrary.com]

with $\tau = 1, \dots, S \cdot T$. The demeaned continuously compounded intraday return is then obtained as $r_\tau = 100 \times \left[\tilde{r}_\tau - (1/(S \cdot T)) \sum_{\tau=1}^{S \cdot T} \tilde{r}_\tau\right]$, where $\tilde{r}_\tau = [\log P_\tau - \log P_{\tau-1}]$.[4]

We then model the stochastic evolution of the intraday asset return r_τ via

$$r_\tau = \sqrt{h_\tau}\eta_\tau, \text{ where } h_\tau = \text{Var}(r_\tau|\mathcal{F}_{\tau-1}), \tag{9}$$

with $\mathcal{F}_\tau = \{r_\tau, r_{t-\tau}, \cdots\}$ and $\eta_\tau \overset{iid}{\sim} F(0,1)$, where $F(0,1)$ refers to a known parametric distribution with zero mean and unit variance. Popular candidates are the normal and the standardized Student's t distribution.

We follow Engle and Sokalska (2012) in assuming a mixed frequency three-component structure for the log-volatility process in order to capture the strong persistence and periodicity of the intraday volatility dynamics:

$$h_\tau = \exp\{\omega_\ell + z_\tau + l_t\}. \tag{10}$$

The period-specific intercepts ω_ℓ capture the well-known u-shaped periodicity in intraday volatilities (the "volatility smile"; see, e.g., Andersen & Bollerslev, 1997) and z_τ and l_t are both short-memory latent volatility components, which are realized at frequencies τ and t. More precisely, z_τ takes new values every period τ, while l_t changes its value every S periods and stays constant for the next $S-1$ periods, until it changes again. Note that, although being driven by short-memory stochastic processes, the mixed-frequency GAS approach is able to generate long-memory type of dependence patterns at the intraday frequency by aggregating independent dynamic stochastic volatility components at different frequencies (see, e.g., Corsi, 2009; Granger, 1980). The dynamics of the three volatility components are schematically illustrated in Figure 1.

[4]Note that we skip the index i for the institution for notational convenience. Also note that we do not model the mean dynamics of the intraday returns, since the data set illustrated in Section 4 does not show significant serial correlation in the return levels.

We assume a GAS-driven autoregressive framework for the stochastic evolution of z_τ and l_t over time, that is,

$$z_\tau = \alpha_1^{(z)} z_{\tau-1} + \alpha_2^{(z)} \xi_{\tau-1}^{(z)}, \tag{11}$$

$$l_t = \alpha_1^{(l)} l_{t-1} + \alpha_2^{(l)} \xi_{t-1}^{(l)}, \tag{12}$$

where the innovations $\xi_\tau^{(z)}$ and $\xi_t^{(l)}$ are defined as the scaled scores of log-likelihood contributions at the respective frequencies:

$$\xi_\tau^{(z)} = s_\tau^{(z)} \nabla_\tau^{(z)}, \qquad \nabla_\tau^{(z)} = \frac{\partial \log f(r_\tau|\mathcal{F}_{\tau-1})}{\partial z_\tau}, \tag{13}$$

$$\xi_t^{(l)} = s_t^{(l)} \nabla_t^{(l)},$$
$$\nabla_t^{(l)} = \frac{\partial \log f(r_{(t-1)\cdot S+1}, r_{(t-1)\cdot S+2}, \dots, r_{t\cdot S}|\mathcal{F}_{(t-1)\cdot S})}{\partial l_t}. \tag{14}$$

While the definition of the innovation $\xi_\tau^{(z)}$ in Equation (13) is standard in the context of GAS models, the definition of $\xi_t^{(l)}$ in Equation (14) reflects the mixed frequency structure of the model by taking into account the informational content of all return information at frequency t for the evolution of the process for l_t. We denote the framework as volatility mixed frequency GAS (V-MF-GAS) model.

A typical choice for the scaling coefficients $s_\tau^{(z)}$ and $s_t^{(l)}$ is the square-root of the inverse Fisher information, $s_\tau^{(z)} = (E[(\nabla_\tau^{(z)})^2|\mathcal{F}_{\tau-1}])^{-0.5}$ and $s_t^{(l)} = (E[(\nabla_t^{(l)})^2|\mathcal{F}_{t-1}])^{-0.5}$, which allows for a straight forward analysis of weak stationarity of the stochastic processes for z_τ and l_t. The analytical derivation of the Fisher information is however often problematic for complex stochastic models, such that a unit scaling appears to be an obvious choice in such situations. For the GAS specifications proposed in the following sections, we will employ analytical Fisher scaling whenever possible and unit scaling in all cases where analytical expressions for the Fisher information are not available.

Our basic specification of the V-MF-GAS model (labeled V-MF-GAS-N) assumes a normal distribution for the

conditional return innovation η_τ in Equation (9). The Gaussian log-likelihood contribution is given by

$$\log f(r_\tau|\mathcal{F}_{\tau-1}) = -0.5\log(2\pi) - 0.5\log(h_\tau) - 0.5 r_\tau^2 h_\tau^{-1}. \quad (15)$$

For the scores and Fisher information, we then obtain

$$\nabla_\tau^{(z)} = 0.5\left(r_\tau^2 h_\tau^{-1} - 1\right), \qquad E[(\nabla_\tau^{(z)})^2|\mathcal{F}_{\tau-1}] = 0.5, \quad (16)$$

$$\begin{aligned} \nabla_t^{(l)} &= 0.5\sum_{j=1}^{S}\left(r_{(t-1)\cdot S+j}^2 h_{(t-1)\cdot S+j}^{-1} - 1\right), \\ E[(\nabla_t^{(l)})^2|\mathcal{F}_{t-1}] &= 0.5S. \end{aligned} \quad (17)$$

Since intraday asset return data are typically characterized by heavy tails, it may be reasonable to replace the normal by a standardized Student's t distribution. The Student t log-likelihood contribution is given by

$$\begin{aligned} \log f(r_\tau|\mathcal{F}_{\tau-1}) = {} & \log\Gamma\left(\frac{\nu+1}{2}\right) - \log\Gamma\left(\frac{\nu}{2}\right) \\ & - \frac{1}{2}\log(\nu-2) - \frac{1}{2}\log(h_\tau) \\ & - \left(\frac{\nu+1}{2}\right)\log\left(1 + \frac{r_\tau^2}{(\nu-2)h_\tau}\right), \end{aligned} \quad (18)$$

where ν denotes the d.o.f. parameter. We then obtain

$$\nabla_\tau^{(z)} = \frac{(\nu+1)}{2}\left(1 + \frac{r_\tau^2}{(\nu-2)h_\tau}\right)^{-1}\frac{r_\tau^2}{(\nu-2)h_\tau} - \frac{1}{2}, \quad (19)$$

$$\begin{aligned} \nabla_t^{(l)} = \sum_{j=1}^{S}\Bigg[& \frac{(\nu+1)}{2}\left(1 + \frac{r_{(t-1)\cdot S+j}^2}{(\nu-2)h_{(t-1)\cdot S+j}}\right)^{-1} \\ & \times \frac{r_{(t-1)\cdot S+j}^2}{(\nu-2)h_{(t-1)\cdot S+j}} - \frac{1}{2}\Bigg], \end{aligned} \quad (20)$$

and

$$E[(\nabla_\tau^{(z)})^2|\mathcal{F}_{\tau-1}] = \frac{\nu}{2(\nu+3)}, \qquad E[(\nabla_t^{(l)})^2|\mathcal{F}_{t-1}] = \frac{S\nu}{2(\nu+3)}. \quad (21)$$

The Student's t specification of the V-MF-GAS model is labeled V-MF-GAS-t. Given the GAS innovations defined above, the stochastic processes for z_τ and l_t in Equations (11) and (12) are weakly stationary if $|\alpha_1^{(z)}| < 1$ and $|\alpha_1^{(l)}| < 1$, respectively.

The V-MF-GAS models assume a mixed frequency volatility process where the "long-term" volatility component l_t changes at the daily frequency. Although the daily frequency is in line with the original approach of Engle and Sokalska (2012), the V-MF-GAS framework trivially allows to change the frequency to any desired change point. For example, we could allow for changing volatility levels every hour or every half-day and so on. In fact, we can also estimate the optimal change point by likelihood comparison over several hypothetical values for S (see Section 3.3 for details on the ML parameter estimation of the V-MF-GAS models). Initial estimations, however, showed that a typical ML estimate for the change point is the daily frequency, which led us to fix the frequency of the long-term component l_t to the daily one. This choice is consistent with the work of Engle and Sokalska (2012), offers a good fit to the data (see Section 4), and simplifies model estimation without loss of flexibility.

The literature offers several approaches for modeling the intraday periodicity $\{\omega_\ell\}_{\ell=1}^{S}$: One could estimate all S intercepts individually or apply splines or Fourier transforms in order to save parameters (compare, e.g., Deo et al., 2006; Koopman et al., 2017; Payne, 1996). In our case, the data set comprises S intraday return observations for a total of T trading days. Hence, we can easily estimate all S intercepts individually in order to preserve a maximum of flexibility without unduly increasing overall estimation error.[5]

We finally note that it is also possible to model the autoregressive parameters of the z_τ process periodically as in Rossi and Fantazzini (2015). However, we refrain to follow this approach since it dramatically increases the number of model parameters and an initial investigation did not indicate significant gains in model fit.

3.1.2 | The V-MF-GAS-J Model

It is widely documented that intraday return data may be affected by discrete price jumps induced by unusual news events like earnings surprises. These events cause infrequent large moves in the returns, which tend to cluster together. For example, market crashes can be realized as a series of jumps over a short period of time (see, e.g., Maheu & McCurdy, 2004).

In order to account for intraday price jumps, we extend the V-MF-GAS approach to a mixed GAS-Jump model (labeled as V-MF-GAS-J) based on a compound Poisson jump process in the spirit of Maheu and McCurdy (2004): We decompose the return process into two components, $\epsilon_{1\tau}$ and $\epsilon_{2\tau}$, where $\epsilon_{1\tau}$ represents "normal" news events inducing smooth price changes, and $\epsilon_{2\tau}$ denotes news "surprises," which cause relatively infrequent large price changes. Under the basic assumption of Gaussian distributed return innovations, we obtain

$$r_\tau = \epsilon_{1\tau} + \epsilon_{2\tau}, \quad (22)$$

where

$$\epsilon_{1\tau} = \sqrt{h_\tau}\, e_\tau, \; e_\tau \overset{iid}{\sim} N(0,1), \quad (23)$$

[5]Note that each ω_ℓ is estimated using roughly T observations (e.g., $T = 2265$ in the empirical application; see Section 4).

$$\epsilon_{2\tau} = \sum_{j=1}^{n_\tau} c_{j\tau} - \theta\lambda_\tau,\ c_{j\tau} \overset{iid}{\sim} N(\theta, \delta^2), \tag{24}$$

and $n_\tau|\mathcal{F}_{\tau-1} \sim Poi(\lambda_\tau)$ with time-varying news arrival intensity λ_τ. Here, we assume that the conditional volatility h_τ is driven by the V-MF-GAS process of the previous section. Under Gaussian innovations e_τ and $c_{j\tau}$, we obtain

$$f(r_\tau|n_\tau = j, \mathcal{F}_{\tau-1}) \sim N\left(\theta(j - \lambda_\tau), h_\tau + j\delta^2\right). \tag{25}$$

The corresponding volatility forecast is given by $\text{Var}(r_\tau|\mathcal{F}_{\tau-1}) = h_\tau + \lambda_\tau(\delta^2 + \theta^2)$.

We model the jump intensity by an autoregressive GAS process, where

$$\lambda_\tau = \exp\{\tilde{f}_\tau\}$$
$$\tilde{f}_\tau = \phi_0 + \phi_1\tilde{f}_{\tau-1} + \phi_2\xi_{\tau-1}^{(j)},$$

with

$$\xi_\tau^{(j)} = s_\tau^{(j)}\nabla_\tau^{(j)}, \qquad \nabla_\tau^{(j)} = \frac{\partial \log f(r_\tau|\mathcal{F}_{\tau-1})}{\partial \tilde{f}_\tau}.$$

We then obtain the likelihood contribution

$$\begin{aligned} f(r_\tau|\mathcal{F}_{\tau-1}) &= \sum_{j=0}^{\infty} f(r_\tau, n_\tau = j|\mathcal{F}_{\tau-1}) \\ &= \sum_{j=0}^{\infty} \frac{\exp\{-\lambda_\tau\}\lambda_\tau^j}{j!\sqrt{2\pi(h_\tau + j\delta^2)}} \exp \\ &\quad \left\{-\frac{(r_\tau + \theta\lambda_\tau - \theta j)^2}{2(h_\tau + j\delta^2)}\right\}. \end{aligned} \tag{26}$$

The jump-adjusted scores are given by

$$\begin{aligned} \nabla_\tau^{(z)} &= \frac{h_\tau}{f(r_\tau|\mathcal{F}_{\tau-1})}\sum_{j=0}^{\infty} f(r_\tau, n_\tau = j|\mathcal{F}_{\tau-1}) \\ &\quad \times\left[\frac{(r_\tau + \theta\lambda_\tau - \theta j)^2}{2(h_\tau + j\delta^2)^2} - \frac{1}{2(h_\tau + j\delta^2)}\right], \\ \nabla_t^{(l)} &= \sum_{j=1}^{S} \nabla_{(t-1)\cdot S+j}^{(z)}, \\ \nabla_\tau^{(j)} &= \frac{\lambda_\tau}{f(r_\tau|\mathcal{F}_{\tau-1})}\sum_{j=0}^{\infty} f(r_\tau, n_\tau = j|\mathcal{F}_{\tau-1}) \\ &\quad \times\left[\left[\frac{j}{\lambda_\tau} - 1\right] - \frac{(r_\tau + \theta\lambda_\tau - \theta j)\theta}{h_\tau + j\delta^2}\right]. \end{aligned}$$

The infinite sums are truncated at $j = 20$ for likelihood evaluation.[6] Since it appears difficult to derive a closed-form expression for the Fisher information under the V-MF-GAS-Jump framework, we follow the standard approach in the literature and set all scaling coefficients to one ($s_\tau^{(z)} = s_t^{(l)} = s_\tau^{(j)} = 1$). The resulting jump model is labeled V-MF-GAS-N-J.

[6] In our empirical application, we seldom encountered nonzero probability mass for more the 10 jumps (see also Maheu & McCurdy, 2004, for a similar truncation). Our results also appear to be robust to increasing truncation limits.

While the V-MF-GAS-N-J model builds on Gaussian return innovations in the spirit of Maheu and McCurdy (2004), it appears natural to replace the normal in Equation (25) by its Student's t analog. While the resulting V-MF-GAS-t-J specification is straightforward to implement, the practical estimation turned out to be unstable for the majority of the 378 time series in our empirical application (see Section 4) with frequent convergence problems during the numerical optimization of the log-likelihood. We attribute this instability to problems with model identification: both the jump process and the Student t innovations account for the heavy tails of the intraday return data, and it appears to be hard to discriminate between the contribution of the jump-part and the return innovation part. We therefore focus on Gaussian innovation processes. Details on the Student t jump specification are available upon request.

3.2 | Dependence

3.2.1 | The C-MF-GAS Model

We employ a dynamic copula approach in order to model the time-varying dependence between the market and the individual asset return. In particular, we follow the Sklar (1959) theorem, which states that the joint conditional distribution can be decomposed into the marginal conditional distribution functions and the conditional copula.

Consider the bivariate time series process $\{r_{i,\tau}, r_{m,\tau}\}_{\tau=1}^{T\cdot S}$, where $r_{\cdot,\tau}$ follows one of the V-MF-GAS models of Section 3.1. The standardized return residuals obtain as

$$\eta_{i,\tau} = \frac{r_{i,\tau}}{\sqrt{Var(r_{i,\tau}|\mathcal{F}_{\tau-1})}} \text{ and } \eta_{m,\tau} = \frac{r_{m,\tau}}{\sqrt{Var(r_{m,\tau}|\mathcal{F}_{\tau-1})}}, \tag{27}$$

with the conditional distribution of $\eta_\tau = (\eta_{i,\tau}, \eta_{m,\tau})'$ given $\mathcal{F}_{\tau-1}$ denoted by

$$\eta_\tau|\mathcal{F}_{\tau-1} \sim F_{\eta_{i,\tau}\eta_{m,\tau}}(\eta_{i,\tau}, \eta_{m,\tau}|\mathcal{F}_{\tau-1}). \tag{28}$$

According to Sklar's theorem, we can now write the joint distribution as

$$F_{\eta_{i,\tau}\eta_{m,\tau}}(\eta_{i,\tau}, \eta_{m,\tau}|\mathcal{F}_{\tau-1}) = C(u_{i,\tau}, u_{m,\tau}; \theta_\tau|\mathcal{F}_{\tau-1}), \tag{29}$$

where $C(\cdot)$ denotes a conditional copula function with n-dimensional dynamic dependence parameter $\theta_\tau = (\theta_{1,\tau}, \ldots, \theta_{n,\tau})'$ and corresponding copula density $c(\cdot)$. The copula is defined as a distribution function on the two-dimensional hypercube with uniform marginals. The arguments $u_{i,\tau}$ and $u_{m,\tau}$ of the copula function are obtained by the probability integral transform

$$u_{i,\tau} = F_{\eta_{i,\tau}}(\eta_{i,\tau}|\mathcal{F}_{\tau-1}) \text{ and } u_{m,\tau} = F_{\eta_{m,\tau}}(\eta_{m,\tau}|\mathcal{F}_{\tau-1}), \tag{30}$$

with $F_{\eta_{\cdot,\tau}}(\eta_{\cdot,\tau}|\mathcal{F}_{\tau-1})$ being conditional distribution functions given $\mathcal{F}_{\tau-1}$, as implied by the volatility models for $r_{i,\tau}$ and $r_{m,\tau}$. For the V-MF-GAS-N and V-MF-GAS-t models,

the marginal distributions $F_{\eta_{\cdot,\tau}}$ are standard Gaussian and Student's t, respectively (compare the model specifications in Section 3.1.1). For the jump specifications, the distributions obtain as mixtures over the stochastic numbers of jumps (see Equation 26) and can be approximated by the empirical cdf of the estimated residual series $\{\hat{\eta}_{i,\tau}\}$ and $\{\hat{\eta}_{m,\tau}\}$ obtained after ML estimation of the model parameters.

Empirical applications of conditional copula models for daily asset returns typically report evidence of long-memory type of dependence structures for the dependence parameters (see, e.g., Janus et al., 2014; Grossmass & Poon, 2015). We therefore employ the MF-GAS process of Section 3.1 in order to model the copula dynamics. Let

$$\theta_\tau = g(\psi_\tau), \qquad \text{with} \tag{31}$$

$$\psi_\tau = \tilde{\omega}_\ell + \tilde{z}_\tau + \tilde{l}_t, \tag{32}$$

where $\tilde{\omega}_\ell = (\tilde{\omega}_{1,\ell}, \dots, \tilde{\omega}_{n,\ell})'$, $\tilde{z}_\tau = (\tilde{z}_{1,\tau}, \dots, \tilde{z}_{n,\tau})'$ and $\tilde{l}_t = (\tilde{l}_{1,\tau}, \dots, \tilde{l}_{n,\tau})'$ are n-dimensional dynamic intraday and daily dependence components and g is an n-dimensional monotonously increasing function, which maps the dependence components into the domain of the copula parameters. Note that we include periodic constants $\tilde{\omega}_\ell$ in order to account for potential seasonality in the copula parameters. Let

$$\tilde{z}_{j,\tau} = \tilde{\alpha}^{(z)}_{j,1}\tilde{z}_{j,\tau-1} + \tilde{\alpha}^{(z)}_{j,2}\tilde{\xi}^{(z)}_{j,\tau-1} \tag{33}$$

$$\tilde{l}_{j,t} = \tilde{\alpha}^{(l)}_{j,1}l_{j,t-1} + \tilde{\alpha}^{(l)}_{j,2}\tilde{\xi}^{(l)}_{j,t-1}, \tag{34}$$

for $j = 1, \dots, n$. The GAS innovations $\tilde{\xi}^{(z)}_{j,\tau}$ and $\tilde{\xi}^{(l)}_{j,t}$ are defined analogously to Equations (13) and (14):

$$\xi^{(\tilde{z})}_{j,\tau} = s^{(\tilde{z})}_{j,\tau}\nabla^{(\tilde{z})}_{j,\tau}, \qquad \nabla^{(\tilde{z})}_{j,\tau} = \frac{\partial \log c(u_\tau|\mathcal{F}_{\tau-1})}{\partial \tilde{z}_{j,\tau}}, \tag{35}$$

$$\xi^{(\tilde{l})}_{j,t} = s^{(\tilde{l})}_{j,t}\nabla^{(\tilde{l})}_{j,t}, \qquad \nabla^{(\tilde{l})}_{j,t} = \frac{\partial \log c(u_{(t-1)\cdot S+1}, u_{(t-1)\cdot S+2}, \dots, u_{t\cdot S}|\mathcal{F}_{(t-1)\cdot S})}{\partial \tilde{l}_{j,t}}, \tag{36}$$

with $u_\tau = (u_{i,\tau}, u_{m,\tau})'$. According to the previous section, we denote the framework as Copula(C)-MF-GAS.

We investigate three popular copula functions, which account for different kinds of dependencies:

1. The bivariate Gaussian copula with time-varying correlation parameter $\theta_\tau = \rho_\tau \in (-1, 1)$. The copula density is given by

$$c(u_{i,\tau}, u_{m,\tau}|\mathcal{F}_{\tau-1}) = \frac{1}{\sqrt{1-\rho_\tau^2}} \exp\left\{-\frac{\rho_\tau^2(x_{i,\tau}^2 + x_{m,\tau}^2) - 2\rho_\tau x_{i,\tau}x_{m,\tau}}{2(1-\rho_\tau^2)}\right\}, \tag{37}$$

where $x_{i,\tau} = \Phi^{-1}(u_{i,\tau})$ and $x_{m,\tau} = \Phi^{-1}(u_{m,\tau})$ with $\Phi^{-1}(\cdot)$ denoting the inverse of the Gaussian cdf. We define the link function g as

$$\rho_\tau = g(\psi_\tau) = \frac{\exp(\psi_\tau) - 1}{\exp(\psi_\tau) + 1} \tag{38}$$

and obtain

$$\nabla^{(\tilde{z})}_\tau = \frac{\rho_\tau(1 - x_{i,\tau}^2 - x_{m,\tau}^2) + (1+\rho_\tau^2)x_{i,\tau}x_{m,\tau} - \rho_\tau^3}{(\rho_\tau^2 - 1)^2}\,\dot{\rho}_\tau, \tag{39}$$

$$\nabla^{(\tilde{l})}_t = \sum_{j=1}^{S} \nabla^{(\tilde{z})}_{(t-1)\cdot q+j}, \tag{40}$$

where $\dot{\rho}_\tau = \partial\rho_\tau/\partial\tilde{z}_\tau$. We use the square-root of the inverse Fisher information for the scaling of the GAS innovations with the according formulas given in Appendix A.

2. The bivariate Student's t copula with time-varying correlation parameter $\theta_\tau = \rho_\tau \in (-1, 1)$ and time-constant degrees of freedom parameter $\kappa > 4$. The copula density is given by

$$c(u_{i,\tau}, u_{m,\tau}|\mathcal{F}_{\tau-1}) = \frac{\Gamma\left(\frac{\kappa+2}{2}\right)\Gamma\left(\frac{\kappa}{2}\right)}{\Gamma\left(\frac{\kappa+1}{2}\right)\sqrt{1-\rho_\tau^2}} \cdot \frac{\left[1 + \kappa^{-1}(1-\rho_\tau^2)^{-1}(x_{i,\tau}^2 + x_{m,\tau}^2 - 2\rho_\tau x_{i,\tau}x_{m,\tau})\right]^{-(\kappa+2)/2}}{\left[(1 + x_{i,\tau}^2/\kappa)(1 + x_{m,\tau}^2/\kappa)\right]^{-(\kappa+1)/2}}, \tag{41}$$

where $x_{i,\tau} = t^{-1}(u_{i,\tau}; \kappa)$ and $x_{m,\tau} = t^{-1}(u_{m,\tau}; \kappa)$ with $t^{-1}(\cdot)$ denoting the inverse of the Student t cdf. The link function g is defined as in Equation (38), and we obtain

$$\nabla^{(\tilde{z})}_\tau = \left(1 - \rho_\tau^2\right)^{-2} \times \left[(1+\rho_\tau^2)(\pi_\tau x_{i,\tau}x_{m,\tau} - \rho_\tau) - \rho_\tau(\pi_\tau x_{i,\tau}^2 + \pi_\tau x_{m,\tau}^2 - 2)\right]\dot{\rho}_\tau, \tag{42}$$

$$\nabla^{(\tilde{l})}_t = \sum_{j=1}^{S} \nabla^{(\tilde{z})}_{(t-1)\cdot q+j}, \tag{43}$$

where

$$\pi_\tau = (\kappa+2)(\kappa+m_\tau)^{-1}, \qquad m_\tau = \left(1-\rho_\tau^2\right)^{-2}\left(x_{i,\tau}^2 + x_{m,\tau}^2 - 2\rho_\tau x_{i,\tau}x_{m,\tau}\right), \qquad \dot{\rho}_\tau = \partial\rho_\tau/\partial\tilde{z}_\tau. \tag{44}$$

We use the square-root of the inverse Fisher information for the scaling of the GAS innovations with the according formulas given in Appendix A.

3. A mixture of Clayton and rotated Clayton copula (labeled CrC Copula) with time-varying copula parameters $\theta_{1\tau} > 0$, $\theta_{2\tau} > 0$ and time-constant mixture weight w

(see, e.g., Eckernkemper, 2018, for an empirical application of this type of copula). The copula density is given by

$$c(u_{i,\tau}, u_{m,\tau}|\mathcal{F}_{\tau-1}) = w \cdot c_1(u_{i,\tau}, u_{m,\tau}|\mathcal{F}_{\tau-1}) + (1-w) \cdot c_2(u_{i,\tau}, u_{m,\tau}|\mathcal{F}_{\tau-1}) \tag{45}$$

with

$$c_1(u_{i,\tau}, u_{m,\tau}|\mathcal{F}_{\tau-1}) = (1+\theta_{1\tau})(u_{i,\tau}u_{m,\tau})^{-1-\theta_{1\tau}}\left(u_{i,\tau}^{-\theta_{1\tau}} + u_{m,\tau}^{-\theta_{1\tau}} - 1\right)^{-\frac{1}{\theta_{1\tau}}-2}, \tag{46}$$

$$c_2(u_{i,\tau}, u_{m,\tau}|\mathcal{F}_{\tau-1}) = c_1(1-u_{i,\tau}, 1-u_{m,\tau}; \theta_{2\tau}). \tag{47}$$

We define the two-dimensional link function g for $\theta_\tau = (\theta_{1\tau}, \theta_{2\tau})'$ as

$$\theta_\tau = (\exp(\psi_{1\tau}), \exp(\psi_{2\tau}))', \tag{48}$$

and we obtain $\nabla_\tau^{(\tilde{z})} = (\nabla_{1,\tau}^{(\tilde{z})}, \nabla_{2,\tau}^{(\tilde{z})})'$ and $\nabla_t^{(\tilde{l})} = (\nabla_{1,t}^{(\tilde{l})}, \nabla_{2,t}^{(\tilde{l})})'$ as

$$\nabla_\tau^{(\tilde{z})} = \begin{bmatrix} \left(w\frac{\partial c_1(u_{i,\tau},u_{m,\tau}|\mathcal{F}_{\tau-1})}{\partial\theta_{1\tau}}\frac{1}{wc_1(u_{i,\tau},u_{m,\tau}|\mathcal{F}_{\tau-1})+(1-w)c_2(u_{i,\tau},u_{m,\tau}|\mathcal{F}_{\tau-1})}\right)\dot{\theta}_{1\tau} \\ \left((1-w)\frac{\partial c_2(u_{i,\tau},u_{m,\tau}|\mathcal{F}_{\tau-1})}{\partial\theta_{2\tau}}\frac{1}{wc_1(u_{i,\tau},u_{m,\tau}|\mathcal{F}_{\tau-1})+(1-w)c_2(u_{i,\tau},u_{m,\tau}|\mathcal{F}_{\tau-1})}\right)\dot{\theta}_{2\tau} \end{bmatrix}, \tag{49}$$

$$\nabla_t^{(\tilde{l})} = \begin{bmatrix} \sum_{j=1}^q \nabla_{1,(t-1)\cdot q+j}^{(\tilde{z})} \\ \sum_{j=1}^q \nabla_{2,(t-1)\cdot q+j}^{(\tilde{z})} \end{bmatrix}, \tag{50}$$

where $\dot{\theta}_{1\tau} = \partial\theta_{1\tau}/\partial\tilde{z}_{1\tau}$ and $\dot{\theta}_{2\tau} = \partial\theta_{2\tau}/\partial\tilde{z}_{2\tau}$. For practical implementation, we set all scaling coefficients for the GAS recursions to one. The copula derivatives in Equation (49) are given in Appendix A.

The Gaussian copula allows for linear dependence while Student's t copula captures both, linear dependence via the correlation coefficient and non-linear symmetric tail dependence via the additional d.o.f. parameter κ. For a given correlation level, the tail dependence increases by decreasing κ, and for a given value of κ, the tail dependence increases with increasing correlation. The mixture copula finally captures both, symmetric and asymmetric tail dependence, where the level of lower-tail (upper-tail) dependence increases monotonically with the CrC copula parameter $\theta_{1\tau}$ ($\theta_{2\tau}$).

Note that our dynamic specification for ψ_τ in Equation (32) allows us to investigate the presence of intraday periodicity in the dynamic correlation and tail-dependence structure. For the Student t copula, we can separately analyze periodic patterns for the correlation process and the d.o.f via allowing the copula parameter κ to vary across intraday periods. In our empirical application in Section 4, we consider the following dynamic copula specifications: (i) the Gaussian copula with GAS-driven correlation and intraday correlation periodicity (labeled C-MF-GAS-G), (ii) Student's t copula with GAS-driven correlation, correlation periodicity, and nonperiodic d.o.f. κ (labeled C-MF-GAS-t_κ), (iii) Student's t copula with GAS-driven correlation, correlation periodicity and periodic d.o.f. κ (labeled C-MF-GAS-t_{κ_ℓ}), and (iv) the CrC copula with periodicity in both GAS-driven copula parameters (labeled C-MF-GAS-CrC).

3.3 | Estimation

We summarize all time-invariant model parameters in the vector $\vartheta = (\vartheta_i, \vartheta_m, \vartheta_c)'$, where $\vartheta_\cdot$ denotes the vector of parameters for the margins (institution and market) and the copula. The parameter vector ϑ is then estimated by maximum likelihood (ML). Asymptotic standard errors are obtained by inverting a numerical approximation of the Hessian at the ML parameter estimates.

As usual in the context of copula models, the parameters are estimated in two steps (compare, e.g., Janus et al., 2014; Hafner & Manner, 2012). In the first step, the parameters of the margins as specified in Section 3.1 are estimated. The corresponding log-likelihoods for the asset and the market obtain as

$$\mathcal{L}_i = \sum_{\tau=1}^{T\cdot S} \log f_{r_{i,\tau}}(r_{i,\tau}; \vartheta_i|\mathcal{F}_{\tau-1}) \text{ and } \mathcal{L}_m = \sum_{\tau=1}^{T\cdot S} \log f_{r_{m,\tau}}(r_{m,\tau}; \vartheta_m|\mathcal{F}_{\tau-1}), \tag{51}$$

with $f_{r_{\cdot,\tau}}$ being Gaussian or Student's t for the V-MF-GAS-N and V-MF-GAS-t models, respectively. For the jump specification, the likelihood contribution is obtained via Equation (26). The log-likelihoods in Equation (51) are maximized over the model parameters of the marginal distributions, ϑ_i and ϑ_m, for all assets and the market separately, using quasi-Newton methods.

In the second step, the parameters of the copula as specified in Section 3.2.1 are estimated. Therefore, we compute the estimated residuals $\hat{\eta}_{i,\tau}$ and $\hat{\eta}_{m,\tau}$ using Equation (27) based on the parameter estimates from the first step. These residuals are then transformed into $\hat{u}_{i,\tau}$ and $\hat{u}_{m,\tau}$ via the probability integral transform based on the (estimated) conditional Gaussian and Student's t distribution functions (V-MF-GAS-N and V-MF-GAS-t models; see Equation 30), or using the empirical cdf of the $\{\hat{\eta}_{i,\tau}\}_{\tau=1}^{T\cdot S}$ for the jump specifications. The remaining model parameters (ϑ_c) for the copula

process are then estimated via maximizing the copula log-likelihood

$$\mathcal{L}_c = \sum_{\tau=1}^{T\cdot S} \log c(\hat{u}_{i,\tau}, \hat{u}_{m,\tau}; \vartheta_c | \mathcal{F}_{\tau-1}) \tag{52}$$

using quasi-Newton methods.

4 | EMPIRICAL APPLICATION

4.1 | Data

We now apply the proposed model specifications in order to analyze the dynamics of volatilities, (non)linear dependencies, and (Δ)ECoVaR measures for a data set of the 378 most liquid stocks from the S&P 500 index, which are jointly traded between 2004 and 2012. The comparatively huge database gives us the opportunity to analyze the robustness and reliability of our findings across stocks and industry sectors. An overview on the included stocks and GICS sectors is given in Table S1. The data set comprises 15-min intraday log returns for the period starting at January 2, 2004, and ending on December 31, 2012, covering 2265 trading days and a total of 58,890 intraday trading periods.[7] For the computation of the (Δ)ECoVaR, we take the S&P 500 as the market return.[8]

In the following subsections, we start with a separate analysis of the full sample estimation results for the volatility and copula part of the model. Subsequently, we apply those model specifications with the best in-sample fit in order to analyze the resulting (Δ)ECoVaR measures and provide an out-of-sample (Δ)ECoVaR forecasting application. In all subsections, we provide detailed results for three representative time series: the market return (S&P 500), American Express (AXP), and Microsoft (MSFT). In addition, we also report aggregate results for all 378 time series of the complete data set and the according GICS industry sectors.

4.2 | Volatility

We start with the discussion of the estimation results for the volatility MF-GAS models of Section 3.1. We consider the V-MF-GAS-N, V-MF-GAS-*t*, and the V-MF-GAS-N-J model.

Table 1 reports the full sample ML parameter estimates for the S&P 500, the AXP stock, and the MSFT stock. All estimates are significant at the 1% level. We observe strong persistence of the GAS volatility processes with autoregressive coefficients for the intraday and daily components of up to 0.98 and 0.99, respectively. All processes are weakly stationary and the persistence of the daily volatility component is always higher than its intraday counterpart. The estimates for the V-MF-GAS-N-J model imply persistent jump processes with autoregressive GAS parameters of 0.82 and 0.90 for the S&P 500 and the AXP stock, and 0.45 for the MSFT stock. For AXP and MSFT, we find significantly positive mean parameters of the jump innovations (θ), which induce a slightly positive skewness to the return distribution. For the market return, the estimated innovation mean is significantly negative. The overall best in-sample fit is obtained under the V-MF-GAS-*t* specification, which shows the highest value of the log-likelihood and the lowest value of the Akaike information criterion (AIC). The estimates of the Student *t* d.o.f. parameters are very similar for the three return series and take values of about 6.7, which induce rather heavy tails of the intraday return distributions and significant deviations from normality. The table also reports the R^2 of a regression of the nonperiodic part of the log-volatility $l_\tau + z_\tau$ on the daily component l_τ. The GAS-driven daily volatility level explains up to 94% of the total volatility variation and allows the model to capture the highly persistent volatility dynamics without having to resort to ARFIMA-type dynamics (see also the residual autocorrelation functions in Figure 3).

Figure 2 depicts the estimated log-volatility components $\hat{z}_\tau$ and $\hat{l}_\tau$ together with the three representative return series for the S&P 500 and the AXP and MSFT stocks. The mixed-frequency GAS process for the daily component l_τ generates a smooth long-term volatility pattern that captures a main part of the intraday volatility variation. Under the V-MF-GAS-N model, the estimated nonperiodic log-volatility $\hat{z}_\tau + \hat{l}_\tau$ show various distinguished peaks, which are induced by sudden extreme return innovations entering the GAS recursions. This indicates the presence of jump discontinuities and/or fat-tailed return innovations. Both the V-MF-GAS-N-J and the V-MF-GAS-*t* model account for these abnormal returns as seen by the corresponding volatility plots in the third and fourth row of Figure 2. The forecasts appear smoothest for the AIC-preferred V-MF-GAS-*t* model. The figure also illustrates the problem of jointly identifying discrete return jumps and fat-tailed return innovations as the intraday volatility patterns obtained by the V-MF-GAS-*t* and V-MF-GAS-N-J models appear quite similar. Compared with the jump specification, the Student *t* approach is however more parsimonious in parametrization, more easy to implement, and faster to estimate in practice.

Figure 3 reports sample autocorrelation functions and according 95% Bartlett confidence bounds for the squared intraday returns and the squared standardized martingale

[7] The data have been obtained from www.quantquote.com.

[8] A typical issue with intraday data is the occurrence of missing values. Following common practice, we replace such infrequent data gaps by linear interpolation (see, e.g., Sun et al., 2008).

TABLE 1 Full sample ML parameter estimates for the S&P 500, the AXP stock, and the MSFT stock obtained under the V-MF-GAS-N, V-MF-GAS-*t*, and V-MF-GAS-N-J models

	V-MF-GAS-N			**V-MF-GAS-N-J**			**V-MF-GAS-*t***		
	Market	**AXP**	**MSFT**	**Market**	**AXP**	**MSFT**	**Market**	**AXP**	**MSFT**
$\alpha_1^{(z)}$	0.9254	0.8933	0.8970	0.9861	0.8958	0.8534	0.9575	0.8848	0.8813
	(0.0051)	(0.0058)	(0.0055)	(0.0041)	(0.0087)	(0.0096)	(0.0047)	(0.0078)	(0.0077)
$\alpha_2^{(z)}$	0.0729	0.1028	0.1049	0.1351	0.2066	0.3187	0.1000	0.1672	0.1762
	(0.0026)	(0.0032)	(0.0033)	(0.0073)	(0.0089)	(0.0080)	(0.0040)	(0.0059)	(0.0061)
$\alpha_1^{(l)}$	0.9847	0.9930	0.9884	0.9932	0.9941	0.9793	0.9892	0.9954	0.9864
	(0.0023)	(0.0016)	(0.0021)	(0.0021)	(0.0029)	(0.0038)	(0.0030)	(0.0025)	(0.0037)
$\alpha_2^{(l)}$	0.0741	0.0726	0.0522	0.0176	0.0374	0.0385	0.0973	0.1236	0.1015
	(0.0037)	(0.0034)	(0.0029)	(0.0044)	(0.0022)	(0.0024)	(0.0090)	(0.0078)	(0.0070)
ϕ_0	-	-	-	−0.2263	−0.1191	-0.0164	-	-	-
	-	-	-	(0.0803)	(0.0164)	(0.0031)	-	-	-
ϕ_1	-	-	-	0.8297	0.9008	0.4581	-	-	-
	-	-	-	(0.0924)	(0.0719)	(0.0000)	-	-	-
ϕ_2	-	-	-	0.8566	0.9451	0.9877	-	-	-
	-	-	-	(0.0439)	(0.0053)	(0.0008)	-	-	-
θ	-	-	-	−0.0163	0.0272	0.0041	-	-	-
	-	-	-	(0.0024)	(0.0061)	(0.0029)	-	-	-
δ	-	-	-	0.1374	0.2758	0.2161	-	-	-
	-	-	-	(0.0049)	(0.0137)	(0.0000)	-	-	-
ν	-	-	-	-	-	-	6.6610	6.7215	6.8900
	-	-	-	-	-	-	(0.1694)	(0.1714)	(0.1796)
$\mathcal{L}_i$	35,147.7354	−930.2421	9138.9372	36,711.4379	345.9792	10,389.0839	36,841.4604	847.0650	10,748.6106
AIC	−70,235.4708	1920.4842	−18,217.8744	−73,352.8757	−621.9583	−20,708.1677	−73,620.9208	−1632.1300	−21,435.2213
R^2	0.8913	0.9075	0.7741	0.7835	0.9434	0.8309	0.8629	0.9121	0.7796

Note: Asymptotic standard errors are given in parenthesis. The standard errors are obtained by inverting a numerical approximation of the Hessian at the ML parameter estimates. The reported R^2 statistics are obtained from a regression of the non-periodic part of the log-volatility $l_\tau + z_\tau$ on the daily component l_τ. AIC: Akaike information criterion. $\mathcal{L}_i$: log-likelihood.

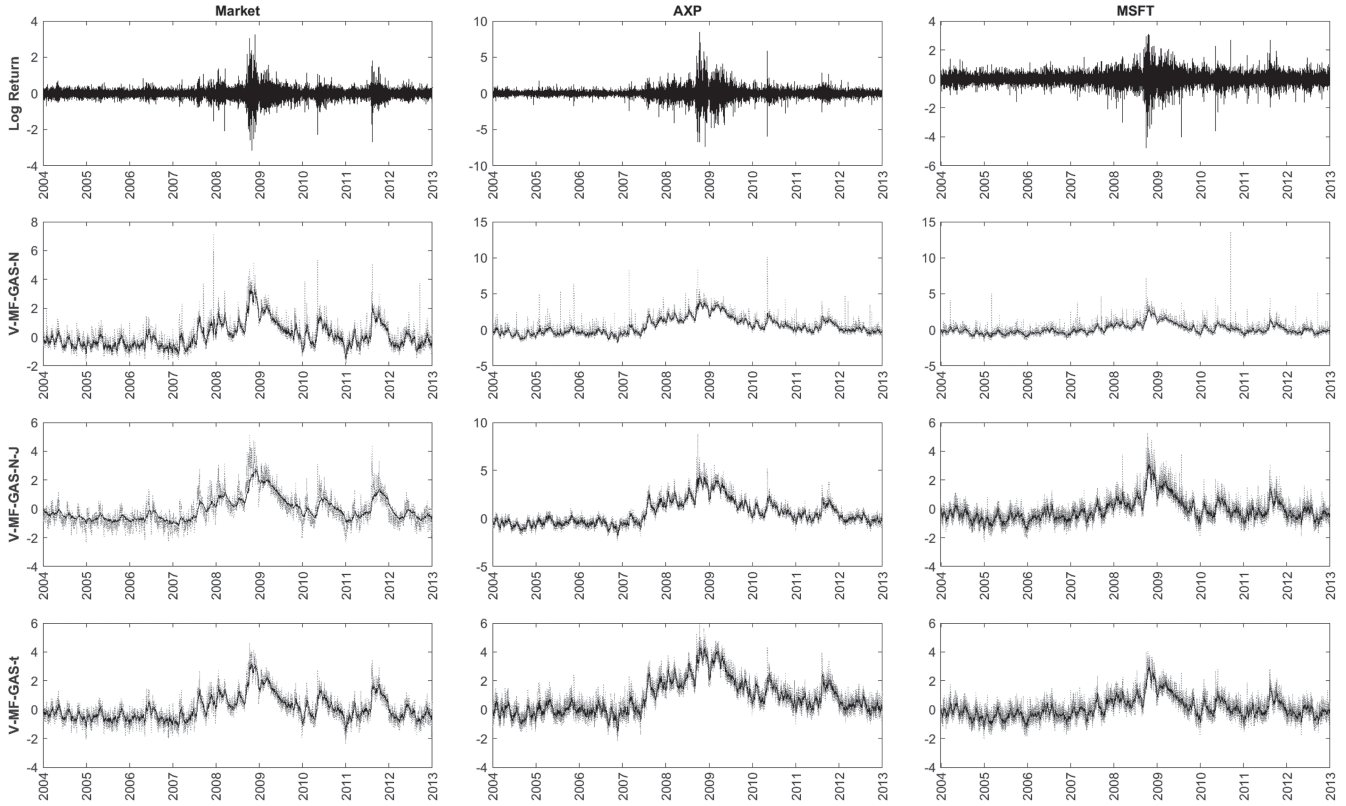

FIGURE 2 Estimated conditional volatility components $\hat{z}_\tau$ and $\hat{l}_\tau$ for the S&P 500, the AXP, and MSFT return series and the V-MF-GAS-N, V-MF-GAS-t, and the V-MF-GAS-N-J models together with the corresponding return series. Dotted grey line: $\hat{z}_\tau + \hat{l}_\tau$; black line: $\hat{l}_\tau$

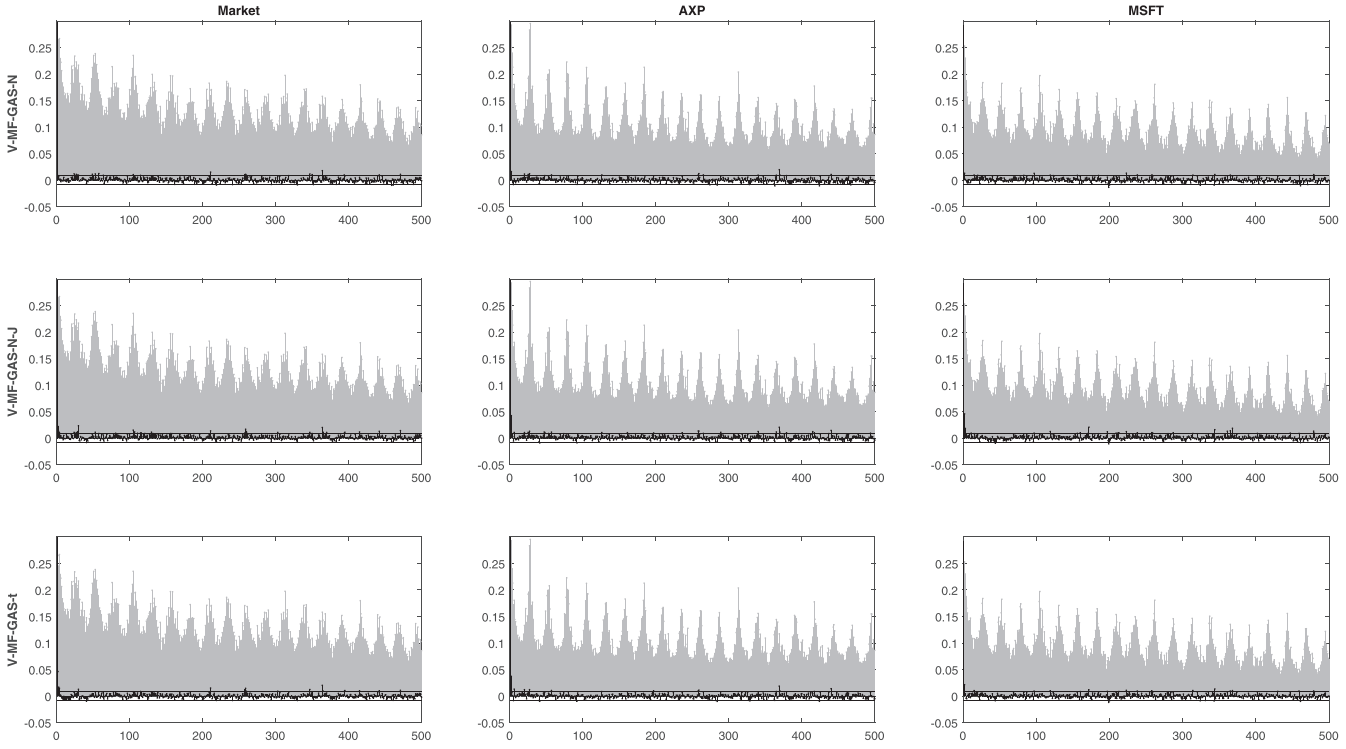

FIGURE 3 Sample autocorrelation functions (500 lags) and according 95% Bartlett confidence bounds for the squared intraday returns of the S&P 500, AXP, and MSFT return series and the squared standardized martingale difference residuals $\eta_\tau^2 = r_\tau^2 / Var(r_\tau | \mathcal{F}_{\tau-1})$, obtained under the V-MF-GAS-N, V-MF-GAS-t and the V-MF-GAS-N-J models

difference residuals $\hat{\eta}_\tau^2 = r_\tau^2 / \widehat{Var}(r_\tau|\mathcal{F}_{\tau-1})$. Under the null of correctly specified volatility dynamics, the squared residuals should be serially uncorrelated. The reported sample autocorrelations are close to zero for all return series and volatility models, which indicates that the three V-MF-GAS models successfully account for the strong persistence of the intraday return variation. At the 1% significance level, Ljung–Box tests still reject the null of zero autocorrelation for the V-MF-GAS-N-J (Market, AXP, and MSFT) and V-MF-GAS-*t* (Market and AXP) models. These test results should however not be overinterpreted because the significance of the test statistics is driven by a few peaks of the ACF. The sample size of 58,890 intraday trading periods induces tight confidence regions for the autocorrelation functions under the null such that infrequent violations of the confidence bands appear rather naturally and can be taken as evidence against overfitting the sample ACF of the data.

We now turn to the discussion of the estimation results for the complete set of 379 intraday return series. The left panel of Table 2 reports aggregate results for the obtained log-likelihood values, AICs and Ljung–Box tests on serial correlation in the squared martingale difference residuals. For the log-likelihoods and the AICs, the table reports the absolute numbers and the percentage of cases, where the respective model is selected. For the Ljung–Box test, the absolute number and the percentage of rejections at the 1% significance level is reported. Both the log-likelihood and the AIC criterion select the V-MF-GAS-*t* approach as the best fitting model for all 378 return series. The jump specification is second-best in 379 and 378 out of 379 cases. Keeping in mind that the total sample size amounts to 58,890 observations, the partly significant Ljung–Box autocorrelation test results indicate an overall good performance in fitting the volatility dynamics while avoiding an overfitting of the sample ACF. The best results are obtained under the V-MF-GAS-N model (21.4% rejections of the null) followed by the V-MF-GAS-*t* (61.5% rejections) and the V-MF-GAS-N-J model (69.1% rejections). The relatively poor performance of the Student *t* and the jump model is not completely unexpected. Liesenfeld and Richard (2003), for example, report similar findings for a Student *t* SV specification. Under the jump and the Student *t* likelihood, extreme (and possibly clustered) observations are effectively down-weighted, resulting in a reduced fit to the autocorrelation structure of the data.

Figure S1 depicts sample averages of the estimated intraday periodicities $\hat{\omega}_\ell$, $\ell = 1, \ldots, 26$, obtained by averaging over the assets within each of the 11 GICS sectors. All estimates are obtained under the V-MF-GAS-*t* model. We observe the typical inverted *U* shape, which appears very similar over the industries for the first 24 periods of the trading day. Only the last two 15-min intervals show significant differences across the sectors with the highest average volatility for the consumer staples and the lowest volatility for the real estate sector.

Based on the estimation results, we can conclude that both the log-likelihood and the AIC criterion select the V-MF-GAS-*t* specification as the best fitting volatility model. We will therefore use this model specification in the next section for modeling the marginal return dynamics within the joint copula framework.

TABLE 2 Aggregate estimation results and model diagnostics for the complete set of 378 assets

	V-MF-GAS			C-MF-GAS			
	N	**N-J**	***t***	**G**	$\boldsymbol{t_\kappa}$	t_{κ_ℓ}	**CrC**
$\mathcal{L}_i$	0	0	379	0	0	377	1
	(0%)	(0%)	(100%)	(0%)	(0%)	(99.7%)	(0.3%)
AIC	0	0	379	0	286	91	1
	(0%)	(0%)	(100%)	(0%)	(75.7%)	(24.1%)	(0.3%)
LB-test	81	262	233	-	-	-	-
	(21.4%)	(69.1%)	(61.5%)				
AD-test	-	-	-	55	11	9	201
				(14.6%)	(2.9%)	(2.4%)	(53.2%)

Note: The left panel reports aggregate results for the obtained log-likelihood values ($\mathcal{L}_i$), AICs, and Ljung–Box (LB) tests on serial correlation in the squared martingale difference residuals for the V-MF-GAS-N-, V-MF-GAS-N-J-, and V-MF-GAS-*t* models. For the log-likelihoods and the AICs, the table reports the absolute numbers and the percentage of cases, where the respective model is selected. For the LB tests, the absolute number and the percentage of rejections at the 1% significance level is reported. The right panel reports analog $\mathcal{L}_i$ and AIC results for the C-MF-GAS-G, C-MF-GAS-t_κ, C-MF-GAS-t_{κ_ℓ}, and C-MF-GAS-CrC models. *AD*-test: Number (percentage) of rejections for the Anderson–Darling (AD) test of the null of independence of the Rosenblatt transformed $\eta_{i,\tau}$ and $\eta_{m,\tau}$ residuals, that is, the null of correct specification of the dependence structure (see Manner & Reznikova, 2012).

TABLE 3 Full sample ML parameter estimates for the bivariate asset- market relationships of the AXP stock and the MSFT stock obtained under the C-MF-GAS-G, C-MF-GAS-t_κ, C-MF-GAS-t_{κ_ℓ}, and C-MF-GAS-CrC models

	C-MF-GAS-G		C-MF-GAS-t_κ		C-MF-GAS-t_{κ_ℓ}		C-MF-GAS-CrC	
	AXP	MSFT	AXP	MSFT	AXP	MSFT	AXP	MSFT
$\alpha_{1,1}^{(z)}$	0.9213	0.8711	0.9129	0.8853	0.9137	0.8811	0.9016	0.9030
	(0.0141)	(0.0264)	(0.0173)	(0.0263)	(0.0174)	(0.0262)	(0.0475)	(0.0423)
$\alpha_{1,2}^{(z)}$	-	-	-	-	-	-	0.8737	0.7327
	-	-	-	-	-	-	(0.0661)	(0.1144)
$\alpha_{2,1}^{(z)}$	0.0396	0.0392	0.0450	0.0391	0.0443	0.0379	0.1548	0.1706
	(0.0040)	(0.0046)	(0.0051)	(0.0054)	(0.0051)	(0.0052)	(0.0394)	(0.0418)
$\alpha_{2,2}^{(z)}$	-	-	-	-	-	-	0.1572	0.2236
	-	-	-	-	-	-	(0.0424)	(0.0551)
$\alpha_{1,1}^{(l)}$	0.9811	0.9749	0.9793	0.9752	0.9789	0.9767	0.9811	0.9612
	(0.0055)	(0.0065)	(0.0063)	(0.0071)	(0.0063)	(0.0066)	(0.0077)	(0.0145)
$\alpha_{1,2}^{(l)}$	-	-	-	-	-	-	0.9726	0.9723
	-	-	-	-	-	-	(0.0100)	(0.0120)
$\alpha_{2,1}^{(l)}$	0.0363	0.0337	0.0430	0.0369	0.0425	0.0346	0.1417	0.1628
	(0.0041)	(0.0038)	(0.0051)	(0.0045)	(0.0050)	(0.0041)	(0.0283)	(0.0364)
$\alpha_{2,2}^{(l)}$	-	-	-	-	-	-	0.1571	0.1292
	-	-	-	-	-	-	(0.0293)	(0.0305)
κ	-	-	13.8395	15.1975	-	-	-	-
	-	-	(0.8163)	(0.9871)	-	-	-	-
w	-	-	-	-	-	-	0.4806	0.4994
	-	-	-	-	-	-	(0.0084)	(0.0090)
$\mathcal{L}_i$	13,245.1117	11,337.6059	13,433.0312	11,486.3831	13,458.8492	11,505.7835	12,836.7121	10,954.3373
AIC	−26,430.2233	−22,615.2117	−26,804.0623	−22,910.7662	−26,805.6983	−22,899.5669	−25,551.4242	−21,786.6747
R_1^2	0.7865	0.8013	0.8014	0.8141	0.8015	0.8156	0.8383	0.7380
R_2^2	-	-	-	-	-	-	0.8429	0.7741

Note: The estimates are based on the estimated residuals $\eta_{i,\tau}$ and $\eta_{m,\tau}$ obtained under the AIC preferred V-MF-GAS-t model for the margins. Asymptotic standard errors are given in parenthesis. The standard errors are obtained by inverting a numerical approximation of the Hessian at the ML parameter estimates. The reported R^2 statistics are obtained from a regression of the non-periodic part of the copula parameter $\tilde{l}_\tau + \tilde{z}_\tau$ on the daily component $\tilde{l}_\tau$. R_1^2 and R_2^2 refer to the two time-varying copula parameters of the C-MF-GAS-CrC model. AIC: Akaike information criterion. $\mathcal{L}_i$: log-likelihood.

4.3 | Copula

Table 3 reports the copula estimation results for the bivariate asset-market relationships of AXP and MSFT. All copula estimates discussed in this section are based on the estimated residuals $\eta_{i,\tau}$ and $\eta_{m,\tau}$ obtained under the AIC preferred V-MF-GAS-t model for the margins.[9] We consider (i) the Gaussian copula with GAS-driven correlation and intraday correlation periodicity (labeled C-MF-GAS-G), (ii) Student's t copula with GAS-driven correlation, correlation periodicity and non-periodic d.o.f. κ (labeled C-MF-GAS-t_κ), (iii) Student's t copula with GAS-driven correlation, correlation periodicity and periodic d.o.f. κ (labeled C-MF-GAS-t_{κ_ℓ}), and (iv) the CrC copula with periodicity in both GAS-driven copula parameters (labeled C-MF-GAS-CrC).

The estimates of the autoregressive GAS parameters imply strong persistence of the intraday and daily GAS components with a higher persistence of the daily component for all copula specifications. All processes are weakly stationary and the reported R^2 statistics indicate that about 80% of the total variation of the estimated copula parameters is attributed to the daily component. The estimated d.o.f. parameters of the C-MF-GAS-t_κ model are 13.84 for AXP and 15.20 for MSFT. These values imply significant deviations from the Gaussian copula and indicate the presence of tail dependence between the asset and the market return. The strength of tail dependence is measured by the tail dependence coefficient λ, which is obtained as

$$\lambda = \lim_{q \to 0} P(x_2 \leq F_{x_2}^{-1}(q) | x_1 \leq F_{x_1}^{-1}(q))$$

for a random vector $x = (x_1, x_2)'$, where $\lambda \in (0, 1)$. For Student's t copula models, λ is a function of the d.o.f. parameter and the time-varying correlation coefficient, that is, λ itself varies with time (see, e.g., Embrechts et al., 2015). Under the C-MF-GAS-t_κ model, we obtain for AXP and MSFT an average λ over the estimated time-varying correlations of 0.0762 and 0.0516, respectively, implying a rather low level of tail dependence. This picture changes slightly by turning to the C-MF-GAS-t_{κ_ℓ} specification with periodic

[9]The copula results are found to be robust to alternative choices for the volatility model.

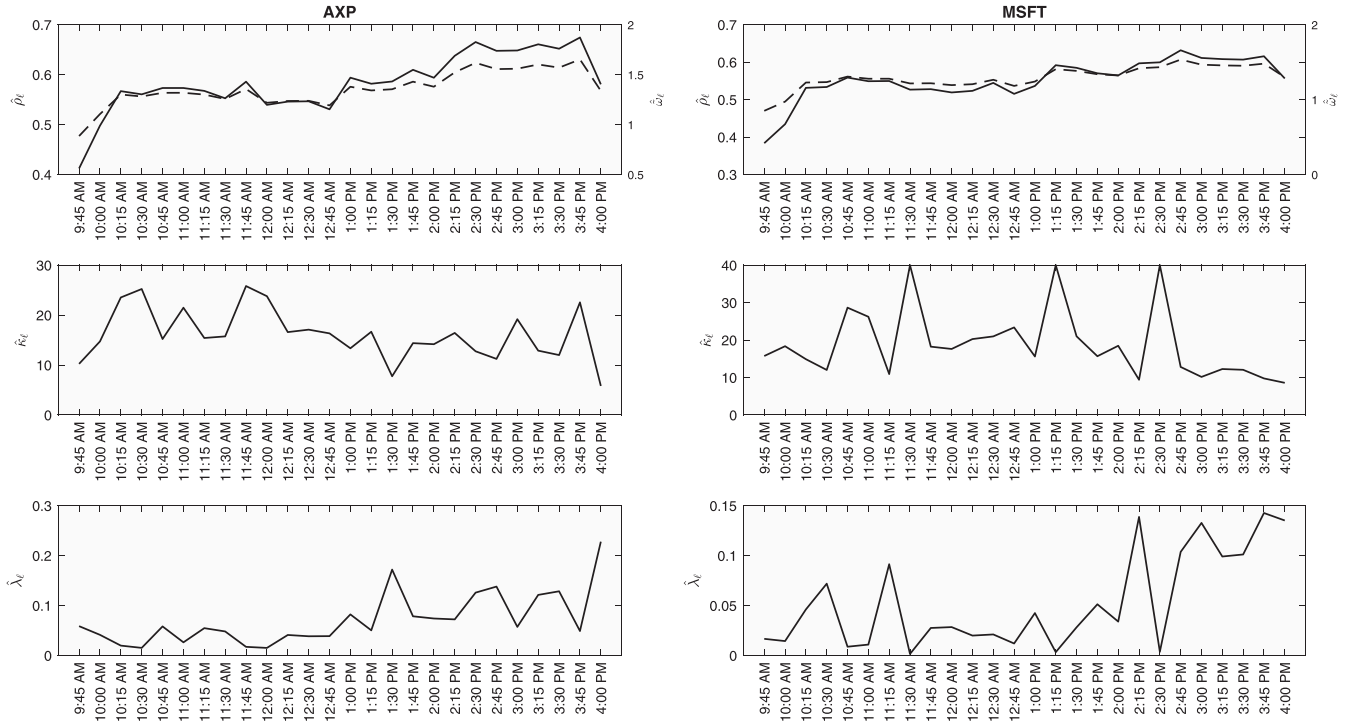

FIGURE 4 Mean correlation estimates $\hat{\rho}_\ell$, averaged over time (together with the according pattern estimates $\hat{\omega}_\ell$), the estimated periodic d.o.f. κ_ℓ, and the mean estimate $\hat{\lambda}_\ell$ obtained by averaging over the time-varying correlations for each of the $\ell = 1, \ldots, 26$ trading periods. All estimates are obtained under the C-MF-GAS-t_{κ_ℓ} model and the V-MF-GAS-t model for the margins. κ estimates >40 are truncated to 40 for better visibility. The Student t copula for more than 40 d.o.f. is virtually undistinguishable from the Gaussian case

d.o.f.: Figure 4 depicts the mean correlation estimates $\hat{\rho}_\ell$, averaged over trading days (together with the according pattern estimates $\hat{\omega}_\ell$), the estimated periodic d.o.f. κ_ℓ, and the mean estimate $\hat{\lambda}_\ell$ obtained by averaging over the time-varying correlations for each of the $\ell = 1, \ldots, 26$ trading periods. We observe a correlation pattern similar to an inverted U shape with less correlation at the beginning than at the end of the active trading hours and an overall increasing correlation trend. We also find an increasing level of tail dependence in the second half of the trading day which is caused by the high correlation level at the end of trading together with an associated decrease of the d.o.f. estimate. The correlation level and the tail dependence measure vary within $(0.4, 0.66)$ and $(0.02, 0.22)$ ($(0.37, 0.64)$ and $(0.00, 0.14)$) for AXP (MSFT), respectively. We analyze the significance of the patterns for AXP and MSFT by Wald tests for the d.o.f. κ_ℓ and periodicity F tests for the time series of correlations and tail dependence measures.[10] All test results are significant at the 1% level with the exception of the d.o.f. estimates for MSFT. The variation of tail dependence over the trading day is particularly pronounced for AXP—a finding that is also reflected by the model fit: The AIC selects the C-MF-GAS-t_κ model for MSFT and the C-MF-GAS-t_{κ_ℓ} model for AXP as the best fitting specifications. The Gaussian and the CrC copula are clearly rejected by the data.

Figure 5 depicts estimates of the time-varying copula GAS processes for the two stocks and the four model specifications. The time series show a high degree of persistence and distinct patterns for AXP and MSFT. The daily copula component evolves smoothly over time and captures a major part of the overall variation in the dependence parameters. We observe frequent negative correlation peaks under the Gaussian copula, which are somewhat dampened by the Student t specifications. Under the CrC copula, the two dependence processes for upper- and lower tail dependence (CRC_1 and CRC_2, respectively) evolve overall similar to the correlations of the Student t specifications.

The aggregated estimation results for the complete set of 378 asset-market combinations are provided in the right panel of Table 2. The C-MF-GAS-t_κ model is AIC preferred for 76% of the time series and the Gaussian and the CrC copulas are clearly rejected by the data. This result is in contrast to the findings of Koopman et al. (2018), who select the Gaussian copula as the best fitting specification within their copula approach on the tick-by-tick frequency.

[10]The Wald test considers the null of equal d.o.f. $\kappa_1 = \kappa_2 = \ldots = \kappa_\ell$. The seasonality test is computed as a standard F test for a regression of the correlations and tail dependence measures on a set of 26 dummies, one dummy for each intraday trading period.

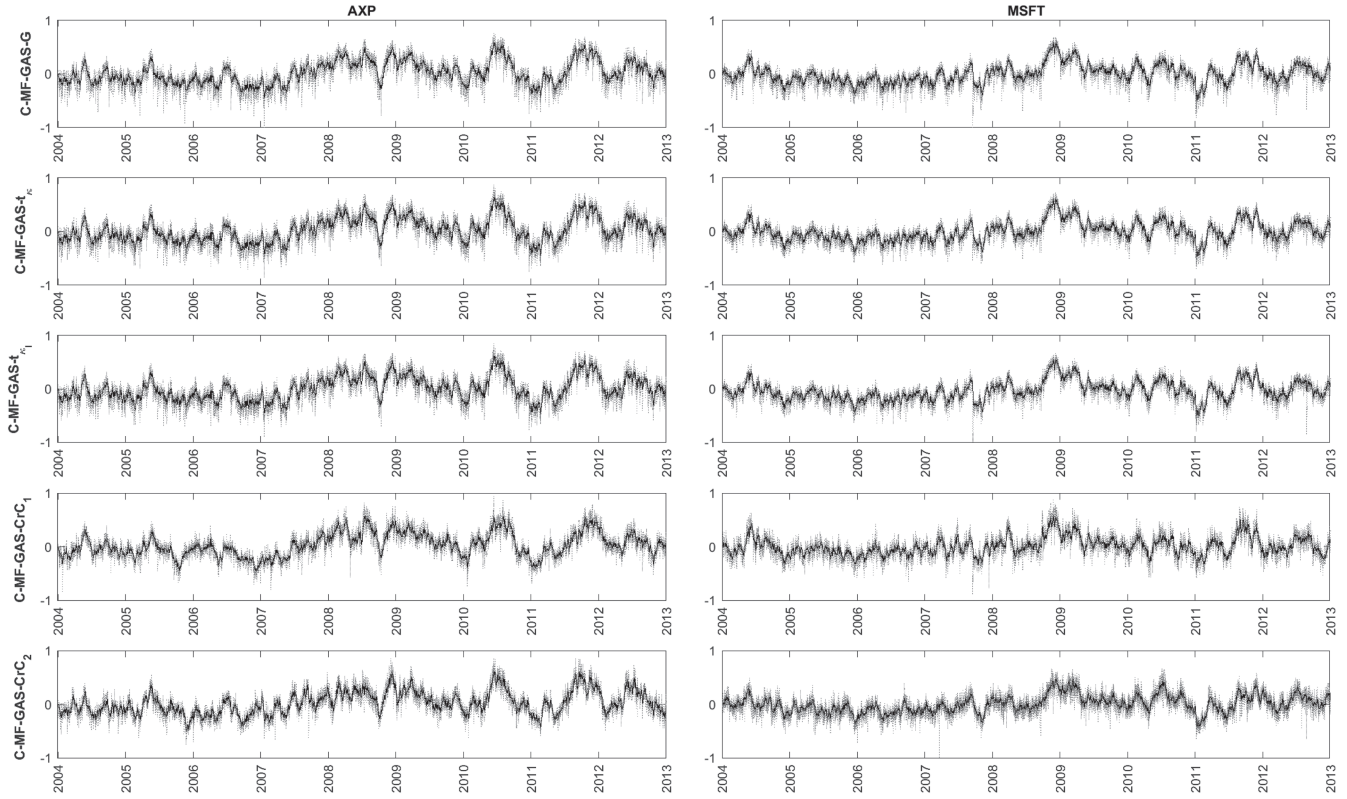

FIGURE 5 Estimates of the time-varying copula GAS parameters for the AXP and MSFT stocks and the C-MF-GAS-G, C-MF-GAS-t_κ, C-MF-GAS-t_{κ_ℓ}, and C-MF-GAS-CrC models. All estimates are obtained under the V-MF-GAS-t model for the margins. Dotted grey line: $\hat{\tilde{z}}_\tau + \hat{\tilde{l}}_t$; black line: $\hat{\tilde{l}}_t$. CrC_i: i-th time-varying parameter of the CrC copula

The C-MF-GAS-t_{κ_ℓ} model is AIC preferred for a subset of 91 assets (about 24%), which are dominated by the Industrials, IT, and Materials sectors. We analyze the in-sample fit of the four copula models via the Anderson–Darling (AD) approach, which tests the null of independence of the Rosenblatt transformed $\eta_{i,\tau}$ and $\eta_{m,\tau}$ residuals, that is, the null of correct specification of the dependence structure (see Manner & Reznikova, 2012). The results are provided in the last line of Table 2. The in-sample residual analyses for the Student t copulas with constant and periodic d.o.f show remarkably good results with 2.9% and 2.4% rejections while the Gaussian and CrC copulas are rejected in 14.6% and even 53.2% of the cases.

Figure S2 reports sample averages of the estimated intraday correlation periodicities $\tilde{\omega}_\ell$, the Student t d.o.f. κ_ℓ, and the average tail-dependence measures λ_ℓ, computed over the assets in each of the 11 industry sectors. All estimates are obtained under the C-MF-GAS-t_{κ_ℓ} model. The correlation pattern show the inverted U shape and increasing correlation trend, which have already been found for the AXP and MSFT stocks. This structure appears consistent over all industry sectors. The correlation "break-downs" at the beginning and the end of the active trading hours are accompanied by comparatively low κ estimates at 4:00 p.m. The high correlation at the afternoon together with a slight tendency of decreasing κ_ℓ results in a common pattern of increasing tail dependence over the trading day. For all industry sectors, the tail-dependence coefficient reaches its maximum at 4 p.m. with a maximum value of 0.16 for the industrial stocks. The positive correlation trend along with the relatively low correlation levels at the beginning and the end of the active trading hours can be explained by the information flow over the 24-h cycle: the rather low correlation level at the start of trading is explained by a relatively large idiosyncratic information component, which is generated by the incorporation of overnight information. During the day however, available pricing-relevant information can directly be processed into stock prices. At the end of active trading, it can be expected that many traders unwind their positions in order to limit the overnight risk. This induces again a rise in the idiosyncratic information component and generates a decrease in the correlations, which induces the U shape (see also the discussion in Koopman et al., 2018).

To summarize our results, we find that the C-MF-GAS-t_κ and C-MF-GAS-t_{κ_ℓ} models provide a good fit to the time-varying and highly persistent intraday dependence processes. We also find an inverted U shaped intraday correlation pattern with a positive common trend over the trading day and a positive trend for the tail-dependence

coefficient. The correlation pattern is consistent with the findings reported by Bibinger et al. (2019) and Koopman et al. (2018).

4.4 | (Δ)ECoVaR

We now select the flexible and in-sample preferred V-MF-GAS-t- and C-MF-GAS-t_{κ_ℓ} copula models for the margins and the dependence structure in order to compute model-based forecasts for the ECoVaR measure. These forecasts are obtained in a straight-forward fashion by applying the approach of Mainik and Schaanning (2014) and Reboredo and Ugolini (2015) as detailed in Section 3 and plugging in the parameter estimates and dynamic volatility and dependence forecasts from the GAS-recursions. In our application, we consider both the ECoVaR (denoted $ECoVaR^{i|m}_{\alpha,\beta,\tau}$) and the ΔECoVaR (denoted $\Delta ECoVaR^{i|m}_{\alpha,\beta,\tau}$) as defined in Equation (5) of Section 2. All forecasts are computed for the VaR levels $\alpha = \beta = 0.05$. The ECoVaR reflects the absolute risk level of the asset in extreme market situations and is therefore closely related to the asset's VaR and the individual volatility dynamics. The ΔECoVaR in contrast measures the exposure of asset i to system-wide distress relative to normal market conditions. It can therefore be interpreted as a measure of the robustness of the asset's VaR to turbulent market conditions. For example, an individual asset (or a portfolio) could feature a high absolute ECoVaR, but a low ΔECoVaR which means that the asset has a high risk level but is rather insensitive to market conditions turning from normal to distress.

4.4.1 | In-sample Analysis

Figure 6 depicts the time-series of in-sample ECoVaR- and ΔECoVaR forecasts for the bivariate asset-market relationships of AXP and MSFT. We observe strong serial dependence for both measures and the ΔECoVaR appears more noisy and less affected by the financial crisis episode of 2008 and 2009 relative to the ECoVaR. Comparing the time-series plots in Figure 6 to the dynamic volatility and dependence estimates in Figures 2 and 5 reveals a strong correspondence of the ECoVaR- and ΔECoVaR dynamics to the volatility and dependence pattern respectively. As expected, we find that episodes of extreme risk like the financial crisis are typically accompanied by high values of the ΔECoVaR (e.g., up to 160% additional ECoVaR risk for AXP relative to a normal market situation). But we also find situations where the ΔECoVaR suddenly drops down while the ECoVaR itself persists on a rather high level (see, e.g., AXP in 2009). Such situations are generated by a sudden decrease in the asset-market dependence

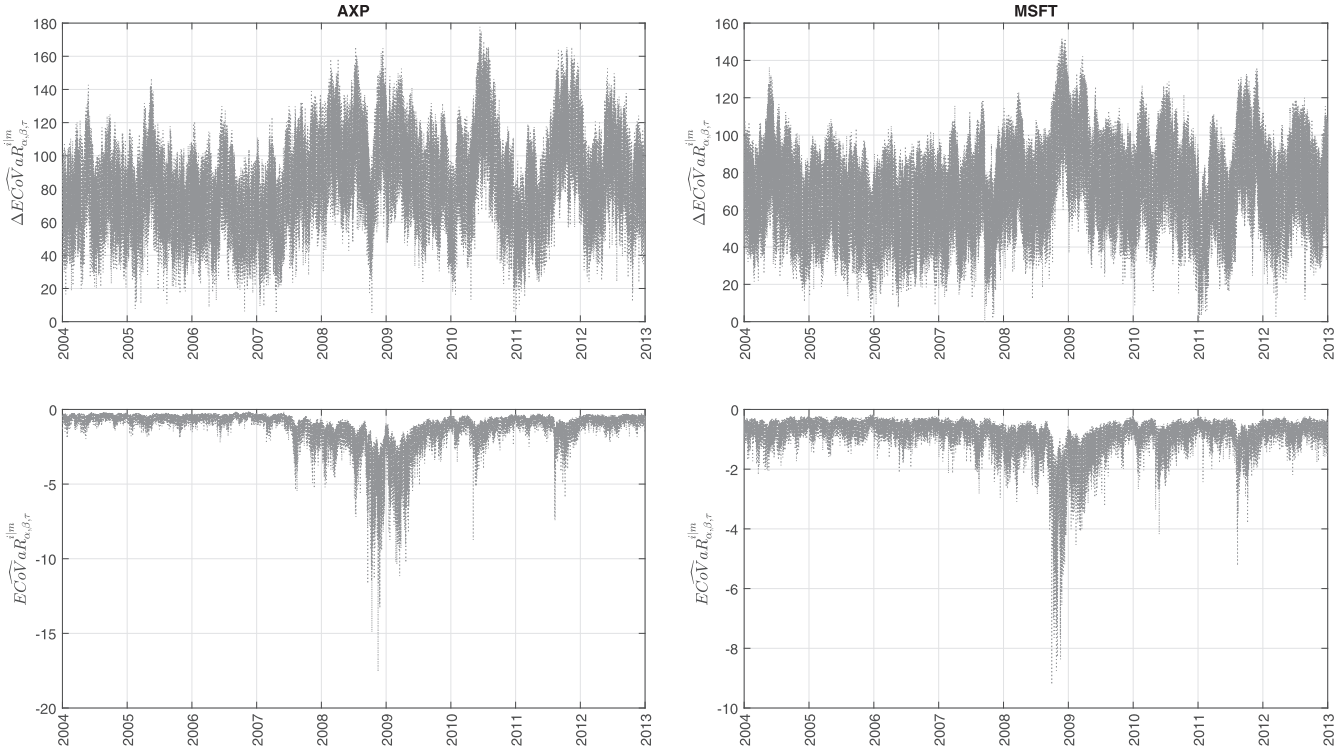

FIGURE 6 In-sample ECoVaR (lower panel) and ΔECoVaR (upper panel) forecasts for the bivariate asset-market relationships of AXP and MSFT. The forecasts are generated under the V-MF-GAS-t- and C-MF-GAS-t_{κ_ℓ} models for the margins and the dependence structure. The computation of the forecasts is based on the copula approach of Mainik and Schaanning (2014) and Reboredo and Ugolini (2015) (see Section 3.1) conditional on the full sample parameter estimates and the copula parameter forecasts from the GAS recursions

while the individual volatility level remains persistently high (compare the dependence pattern in Figure 5).

The dependence of the ECoVaR and ΔECoVaR measures on the intraday volatility and dependence process suggests the existence of intraday seasonalities in the ECoVaR forecasts. These seasonalities are indirectly modeled by the periodicities ω_ℓ and $\tilde{\omega}_\ell$ in the MF-GAS recursions for the volatilities and dynamic copula parameters. The knowledge of such regularities in the ECoVaR measures is important for the active portfolio manager since regular risk-minimizing shiftings of portfolio components due to neglected seasonal effects might induce unnecessary managing costs. Figure 7 depicts mean values of the in-sample ECoVaR and ΔECoVaR estimates for AXP and MSFT averaged over time for each of the 26 intraday periods of the trading day. We find a significant inverse U shape in the ECoVaR estimates and a positive trend for the ΔECoVaR. These patterns are generated by the volatility and correlation periodicities analyzed in Sections 4.2 and 4.3 and confirm the volatility and correlation sensitivity of the ECoVaR and ΔECoVaR measures, respectively.

Figure S3 depicts heat-plots in order to illustrate the variation of the intraday periodicity in the ECoVaR and ΔECoVaR measures over the 378 assets of the complete data set. We observe an overall increasing trend of the ΔECoVaR, which reaches its peak between 2:15 and 3:45 PM and finally fades out at a reduced level at 4:00 PM. The highest ΔECoVaR levels are obtained for the Financial, Industrial , IT , and Material sectors, which show a particularly high risk level at the afternoon hours. Almost all ECoVaR estimates exhibit the inverted U shape generated by the volatility process. The lowest level (highest risk) of the ECoVaR is always obtained at the starting of active trading at 9:45 a.m. The ECoVaR then increases and finally slightly decreases again after 3:45 p.m. The lowest average ECoVaRs are found for the Consumer Staples and Utilities Sectors.

4.4.2 | Out-of-sample Analysis

We now turn to an analysis of the out-of-sample (Δ)ECoVaR forecasting performance. Here, we focus on the importance of modeling the intraday volatility, correlation, and nonlinear dependence patterns. In particular, we investigate the performance of four different models (copula and margins), which are all based on the V-MF-GAS-t- and the C-MF-GAS-t_{κ_ℓ} specifications but account for different aspects of intraday seasonality, that is, seasonality in the volatilities, seasonality in the

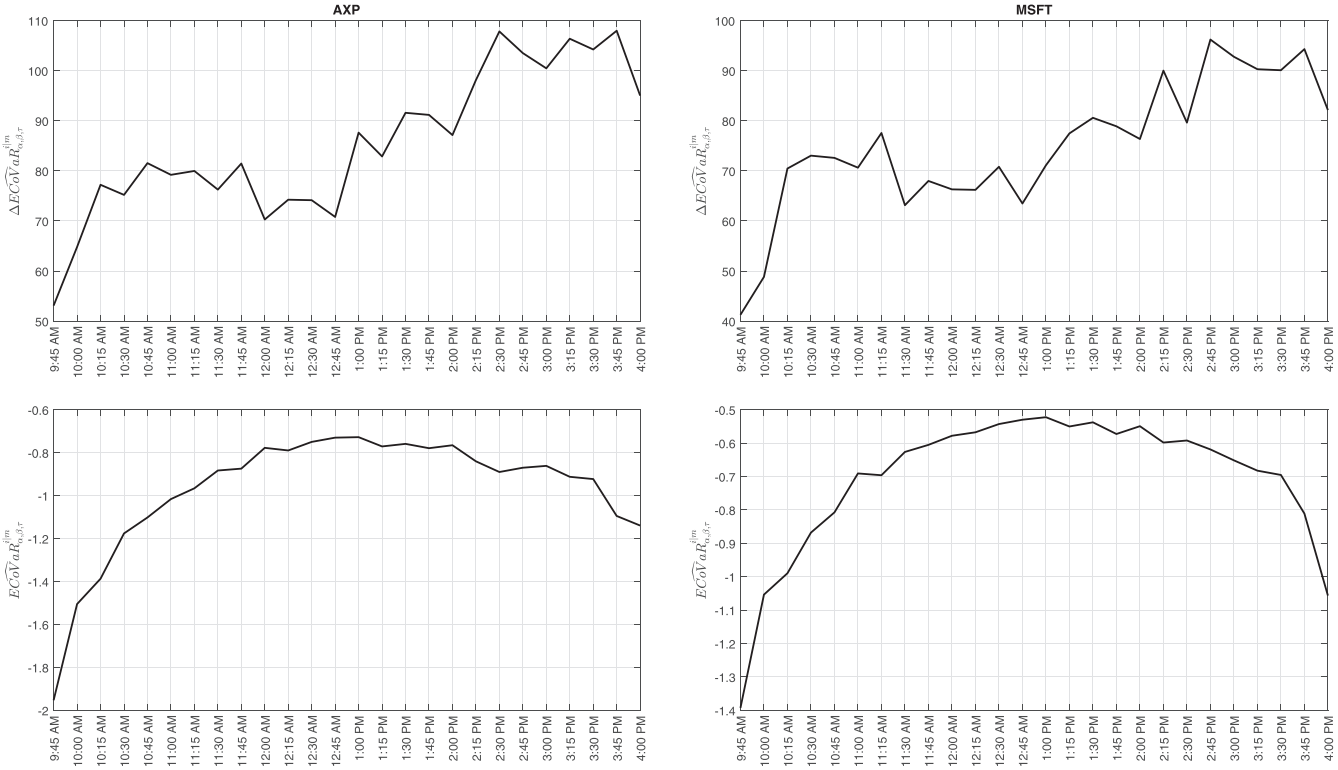

FIGURE 7 Estimated intraday periodicities of the ECoVaR- and ΔECoVaR forecasts for the bivariate asset-market relationships of AXP (left panel) and MSFT (right panel). The estimated periodicities are obtained as sample averages over the $T = 2{,}265$ observations for each intraday period $\ell = 1, \ldots, S = 26$. The forecasts are generated under the V-MF-GAS-t- and C-MF-GAS-t_{κ_ℓ} models for the margins and the dependence structure. The computation of the forecasts is based on the copula approach of Mainik and Schaanning (2014) and Reboredo and Ugolini (2015) (see Section 3.1) conditional on the full sample parameter estimates and the copula parameter forecasts from the GAS recursions

	Margins	Copula	
	Periodicity in Volatility	Periodicity in Correlation	Periodicity in Degrees of Freedom
Model 1	√	√	√
Model 2	√	√	×
Model 3	√	×	×
Model 4	×	×	×

TABLE 4 Overview on the competing model specifications for the out-of-sample forecasting evaluation

correlations, and seasonality in the d.o.f. Table 4 gives an overview on the models.

Because the ECoVaR is a special case of a standard VaR measure, we can readily apply the classical backtesting approaches of the VaR literature in order to compare the out-of-sample performance of various model specifications and periodic structures. Here, we condition on those data points, where the market exceeds its VaR level (see Girardi & Ergün, 2013). In particular, we rely on the standard Kupiec (1995) and Christoffersen (1998) VaR hit-rate tests for those periods, where $r_{m,\tau} \leq VaR^m_{\alpha,\tau}$. We define the "hit sequence" of ECoVaR violations as

$$I^{i|m}_{\tau^*} = \begin{cases} 1 \text{ if } r_{i,\tau^*} \leq ECoVaR^{i|m}_{\alpha,\beta,\tau^*} \\ 0 \text{ else,} \end{cases}$$

where the index τ^* refers to the subsample of observations of size T^*, where $r_{m,\tau} \leq VaR^m_{\alpha,\tau}$. Adequate forecasts of the ECoVaR should satisfy unconditional coverage, that is, $P\left(I^{i|m}_{\tau^*} = 1\right) = \alpha$, which can be tested by the likelihood-ratio (LR) test of Kupiec (1995). A sensible ECoVaR forecasting approach should however also account for the temporal dependence in the ECoVaR estimates. The null of independence in the hit-rate sequence can be tested by the LR independence test proposed by Christoffersen (1998) against the alternative of first order Markov dependence. The conditional coverage test of Christoffersen (1998) then jointly tests the null of unconditional coverage and independence by combining the two individual LR testing procedures.

Unfortunately, it is not possible to design direct backtesting devices in order to investigate the effect of neglected periodicities on the ΔECoVaR. The key problem is that we are not able to observe the "true" ΔECoVaR or any series of hits that can be used for backtesting. We therefore follow an alternative approach and test independence, unconditional coverage and conditional coverage jointly for the two constituents of the ΔECoVaR: the ECoVaR, $ECoVaR^{i|m}_{\alpha,\beta,\tau}$, and the benchmark ECoVaR, $ECoVaR^{i|\text{bench}^m}_{\beta,\tau}$ (see Equation 5). Our joint level-α test is conducted via separate Kupiec (1995) or Christoffersen (1998) hit-rate test for the ECoVaR and the benchmark ECoVaR with Bonferroni correction. The resulting test tends to be conservative with significance level $\alpha^* \leq \alpha$, which accommodates the data-rich environment and the related overfitting issue since the huge intraday sample sizes easily drive the individual test statistics into significance.

We obtain the (Δ)ECoVaR forecasts for all 378 asset-market combinations by splitting the data in the middle and reserving the second half of the time series as the forecasting window. We consider two separate forecasting periods: the period from July 2, 2008, to December 31, 2009, with comparatively high market volatility triggered by the financial crisis, and the relatively calm post-crisis period from January 2, 2010, to December 31, 2012. The two periods together cover a total of $1133 \times 26 = 29458$ periods. Forecasts are generated iteratively with a rolling window scheme[11] and the models are re-estimated at the end of each month. Hence, we obtain overall 1133 forecasts for each of the $S = 26$ intraday periods.

As a natural competitor for our MF-GAS approach, we consider the fractionally integrated GAS (FIGAS) model of Opschoor and Lucas (2019). The model was originally proposed for the joint modeling of daily asset return vectors and realized kernels but is easily adjusted to intraday return series. Let $r^*_\tau = (r_{i,\tau}, r_{m,\tau})'$ denote the bivariate return vector comprising the individual asset return and the market return. Under the FIGAS structure, we obtain

$$r^*_\tau | \mathcal{F}_{\tau-1} \sim t_2(V_\tau, \gamma_\ell),\ V_\tau = \frac{\Omega_\ell}{1-\beta} + \left(1 - \frac{(1-L)^d(1-\phi L)}{1-\beta L}\right) S^*_\tau, \tag{53}$$

where $t_2(V_\tau, \gamma_\ell)$ denotes a bivariate Student's t distribution with zero mean, covariance matrix $V_\tau = (V_{ij,\tau})$, and (possibly) periodic scalar-valued d.o.f. parameter γ_ℓ. L denotes the lag-operator, Ω_ℓ is a p.d. parameter matrix representing the unconditional covariance matrix of r^*_τ, $0 < \beta < 1$, $d \geq \beta$, and S^*_τ is a p.d. GAS innovation matrix with

$$S^*_\tau = S_\tau + V_\tau,\ S_\tau = \underline{S}_\tau \frac{\partial \log f(r^*_\tau | V_\tau)}{\partial V_\tau} \underline{S}'_\tau,$$

where $\underline{S}_\tau = \sqrt{2} V_\tau$. S^*_τ then obtains as

$$S^*_\tau = \omega_\tau r^*_\tau r^{*\prime}_\tau, \text{ with } w_\tau = (\gamma_\ell + 2)(\gamma_\ell - 2 + r^{*\prime}_\tau V^{-1}_\tau r^*_\tau)^{-1}.$$

See Opschoor and Lucas (2019) for details on the model, its derivation, and the ML estimation of the model parameters. The FIGAS accounts for "true" long-memory,

[11] The estimation window size is $1132 \times 26 = 29432$ periods.

TABLE 5 Out-of-sample (Δ)ECoVaR backtesting results: July 2, 2008, to December 31, 2012

		ECoVaR				ΔECoVaR			
Specification (i)									
		Model 1	Model 2	Model 3	Model 4	Model 1	Model 2	Model 3	Model 4
$\alpha = 0.01$	*UC*-test	22	22	17	323	369	372	367	378
		(5.8%)	(5.8%)	(4.5%)	(85.4%)	(97.6%)	(98.4%)	(97.1%)	(100.0%)
	Ind-test	25	22	21	5	57	53	50	66
		(6.6%)	(5.8%)	(5.6%)	(1.3%)	(15.1%)	(14.0%)	(13.2%)	(17.5%)
	CC-test	28	30	26	276	295	298	285	378
		(7.4%)	(7.9%)	(6.9%)	(73.0%)	(78.0%)	(78.8%)	(75.4%)	(100.0%)
$\alpha = 0.05$	*UC*-test	49	48	46	353	377	377	376	378
		(13.0%)	(12.7%)	(12.2%)	(93.4%)	(99.7%)	(99.7%)	(99.5%)	(100.0%)
	Ind-test	50	47	55	21	81	82	83	97
		(13.2%)	(12.4%)	(14.6%)	(5.6%)	(21.4%)	(21.7%)	(22.0%)	(25.7%)
	CC-test	59	60	62	334	317	320	313	378
		(15.6%)	(15.9%)	(16.4%)	(88.4%)	(83.9%)	(84.7%)	(82.8%)	(100.0%)
Specification (ii)									
		Model 1	Model 2	Model 3	Model 4	Model 1	Model 2	Model 3	Model 4
$\alpha = 0.01$	*UC*-test	76	69	50	72	364	370	367	375
		(20.1%)	(18.3%)	(13.2%)	(19.0%)	(96.3%)	(97.9%)	(97.1%)	(99.2%)
	Ind-test	38	42	45	96	114	109	114	309
		(10.1%)	(11.1%)	(11.9%)	(25.4%)	(30.2%)	(28.8%)	(30.2%)	(81.7%)
	CC-test	80	81	76	136	337	340	334	378
		(21.2%)	(21.4%)	(20.1%)	(36.0%)	(89.2%)	(89.9%)	(88.4%)	(100.0%)
$\alpha = 0.05$	*UC*-test	134	119	98	111	375	375	372	377
		(35.4%)	(31.5%)	(25.9%)	(29.4%)	(99.2%)	(99.2%)	(98.4%)	(99.7%)
	Ind-test	86	90	100	156	150	148	152	331
		(22.8%)	(23.8%)	(26.5%)	(41.3%)	(39.7%)	(39.2%)	(40.2%)	(87.6%)
	CC-test	141	128	124	202	351	351	349	378
		(37.3%)	(33.9%)	(32.8%)	(53.4%)	(92.9%)	(92.9%)	(92.3%)	(100.0%)
Specification (iii)									
		Model 1	Model 2	Model 3	Model 4	Model 1	Model 2	Model 3	Model 4
$\alpha = 0.01$	*UC*-test	308	313	319	378	345	351	357	378
		(81.5%)	(82.8%)	(84.4%)	(100.0%)	(91.3%)	(92.9%)	(94.4%)	(100.0%)
	Ind-test	9	9	13	2	20	21	21	213
		(2.4%)	(2.4%)	(3.4%)	(0.5%)	(5.3%)	(5.6%)	(5.6%)	(56.3%)
	CC-test	269	296	317	378	287	310	320	378
		(71.2%)	(78.3%)	(83.9%)	(100.0%)	(75.9%)	(82.0%)	(84.7%)	(100.0%)
$\alpha = 0.05$	*UC*-test	330	335	349	378	358	367	368	378
		(87.3%)	(88.6%)	(92.3%)	(100.0%)	(94.7%)	(97.1%)	(97.4%)	(100.0%)
	Ind-test	28	33	43	16	41	38	46	245
		(7.4%)	(8.7%)	(11.4%)	(4.2%)	(10.8%)	(10.1%)	(12.2%)	(64.8%)
	CC-test	328	331	339	378	330	342	353	378
		(86.8%)	(87.6%)	(89.7%)	(100.0%)	(87.3%)	(90.5%)	(93.4%)	(100.0%)
Specification (iv)									
		Model 1	Model 2	Model 3	Model 4	Model 1	Model 2	Model 3	Model 4
$\alpha = 0.01$	*UC*-test	18	17	22	169	378	376	376	378
		(4.8%)	(4.5%)	(5.8%)	(44.7%)	(100.0%)	(99.5%)	(99.5%)	(100.0%)
	Ind-test	15	21	27	8	44	48	53	213
		(4.0%)	(5.6%)	(7.1%)	(2.1%)	(11.6%)	(12.7%)	(14.0%)	(56.3%)
	CC-test	29	27	38	156	362	351	355	378
		(7.7%)	(7.1%)	(10.1%)	(41.3%)	(95.8%)	(92.9%)	(93.9%)	(100.0%)
$\alpha = 0.05$	*UC*-test	52	50	53	246	378	378	378	378
		(13.8%)	(13.2%)	(14.0%)	(65.1%)	(100.0%)	(100.0%)	(100.0%)	(100.0%)
	Ind-test	49	52	65	39	72	77	82	242
		(13.0%)	(13.8%)	(17.2%)	(10.3%)	(19.0%)	(20.4%)	(21.7%)	(64.0%)
	CC-test	65	67	78	225	370	363	365	378
		(17.2%)	(17.7%)	(20.6%)	(59.5%)	(97.9%)	(96.0%)	(96.6%)	(100.0%)

Note: The table shows the number and percentage of rejections of the unconditional coverage (UC), independence (Ind) and conditional coverage (CC) test for all 378 institutions at the 1% and the 5% significance level. Model 1 to Model 4 refer to the periodic model structures given in Table 4.

TABLE 6 Out-of-sample (Δ)ECoVaR backtesting results: July 2, 2008, to December 31, 2009

		ECoVaR				ΔECoVaR			
Specification (i)									
		Model 1	Model 2	Model 3	Model 4	Model 1	Model 2	Model 3	Model 4
$\alpha = 0.01$	*UC*-test	23	19	18	26	357	354	346	363
		(6.1%)	(5.0%)	(4.8%)	(6.9%)	(94.4%)	(93.7%)	(91.5%)	(96.0%)
	Ind-test	12	8	9	2	36	35	29	42
		(3.2%)	(2.1%)	(2.4%)	(0.5%)	(9.5%)	(9.3%)	(7.7%)	(11.1%)
	CC-test	20	19	18	16	297	295	278	336
		(5.3%)	(5.0%)	(4.8%)	(4.2%)	(78.6%)	(78.0%)	(73.5%)	(88.9%)
$\alpha = 0.05$	*UC*-test	58	52	48	69	366	367	363	374
		(15.3%)	(13.8%)	(12.7%)	(18.3%)	(96.8%)	(97.1%)	(96.0%)	(98.9%)
	Ind-test	33	34	27	4	63	62	57	72
		(8.7%)	(9.0%)	(7.1%)	(1.1%)	(16.7%)	(16.4%)	(15.1%)	(19.0%)
	CC-test	48	39	40	52	337	341	330	363
		(12.7%)	(10.3%)	(10.6%)	(13.8%)	(89.2%)	(90.2%)	(87.3%)	(96.0%)
Specification (ii)									
		Model 1	Model 2	Model 3	Model 4	Model 1	Model 2	Model 3	Model 4
$\alpha = 0.01$	*UC*-test	216	208	204	263	374	375	374	377
		(57.1%)	(55.0%)	(54.0%)	(69.6%)	(98.9%)	(99.2%)	(98.9%)	(99.7%)
	Ind-test	20	22	23	22	61	61	59	88
		(5.3%)	(5.8%)	(6.1%)	(5.8%)	(16.1%)	(16.1%)	(15.6%)	(23.3%)
	CC-test	189	184	179	224	374	374	374	378
		(50.0%)	(48.7%)	(47.4%)	(59.3%)	(98.9%)	(98.9%)	(98.9%)	(100.0%)
$\alpha = 0.05$	*UC*-test	273	270	260	293	375	375	375	377
		(72.2%)	(71.4%)	(68.8%)	(77.5%)	(99.2%)	(99.2%)	(99.2%)	(99.7%)
	Ind-test	54	51	65	57	97	93	104	127
		(14.3%)	(13.5%)	(17.2%)	(15.1%)	(25.7%)	(24.6%)	(27.5%)	(33.6%)
	CC-test	253	245	239	285	376	376	376	378
		(66.9%)	(64.8%)	(63.2%)	(75.4%)	(99.5%)	(99.5%)	(99.5%)	(100.0%)
Specification (iii)									
		Model 1	Model 2	Model 3	Model 4	Model 1	Model 2	Model 3	Model 4
$\alpha = 0.01$	*UC*-test	107	110	128	216	313	321	315	370
		(28.3%)	(29.1%)	(33.9%)	(57.1%)	(82.8%)	(84.9%)	(83.3%)	(97.9%)
	Ind-test	4	3	7	1	6	8	7	57
		(1.1%)	(0.8%)	(1.9%)	(0.3%)	(1.6%)	(2.1%)	(1.9%)	(15.1%)
	CC-test	98	104	123	191	221	226	227	358
		(25.9%)	(27.5%)	(32.5%)	(50.5%)	(58.5%)	(59.8%)	(60.1%)	(94.7%)
$\alpha = 0.05$	*UC*-test	180	183	201	289	355	358	355	377
		(47.6%)	(48.4%)	(53.2%)	(76.5%)	(93.9%)	(94.7%)	(93.9%)	(99.7%)
	Ind-test	22	27	24	10	24	23	26	97
		(5.8%)	(7.1%)	(6.3%)	(2.6%)	(6.3%)	(6.1%)	(6.9%)	(25.7%)
	CC-test	161	166	184	269	278	289	289	372
		(42.6%)	(43.9%)	(48.7%)	(71.2%)	(73.5%)	(76.5%)	(76.5%)	(98.4%)
Specification (iv)									
		Model 1	Model 2	Model 3	Model 4	Model 1	Model 2	Model 3	Model 4
$\alpha = 0.01$	*UC*-test	7	16	5	4	378	378	378	378
		(1.9%)	(4.2%)	(1.3%)	(1.1%)	(100.0%)	(100.0%)	(100.0%)	(100.0%)
	Ind-test	11	10	8	2	20	19	14	56
		(2.9%)	(2.6%)	(2.1%)	(0.5%)	(5.3%)	(5.0%)	(3.7%)	(14.8%)
	CC-test	10	14	8	3	378	378	378	378
		(2.6%)	(3.7%)	(2.1%)	(0.8%)	(100.0%)	(100.0%)	(100.0%)	(100.0%)
$\alpha = 0.05$	*UC*-test	31	40	29	23	378	378	378	378
		(8.2%)	(10.6%)	(7.7%)	(6.1%)	(100.0%)	(100.0%)	(100.0%)	(100.0%)
	Ind-test	34	35	37	10	41	42	42	75
		(9.0%)	(9.3%)	(9.8%)	(2.6%)	(10.8%)	(11.1%)	(11.1%)	(19.8%)
	CC-test	35	42	28	16	378	378	378	378
		(9.3%)	(11.1%)	(7.4%)	(4.2%)	(100.0%)	(100.0%)	(100.0%)	(100.0%)

Note: The table shows the number and percentage of rejections of the unconditional coverage (UC), independence (Ind), and conditional coverage (CC) test for all 378 institutions at the 1% and the 5% significance level. Model 1 to Model 4 refer to the periodic model structures given in Table 4.

TABLE 7 Out-of-sample (Δ)ECoVaR backtesting results: January 2, 2010, to December 31, 2012

		ECoVaR				ΔECoVaR			
Specification (i)									
		Model 1	Model 2	Model 3	Model 4	Model 1	Model 2	Model 3	Model 4
$\alpha = 0.01$	*UC*-test	5	13	9	327	251	258	244	375
		(1.3%)	(3.4%)	(2.4%)	(86.5%)	(66.4%)	(68.3%)	(64.6%)	(99.2%)
	Ind-test	11	14	15	5	43	47	44	58
		(2.9%)	(3.7%)	(4.0%)	(1.3%)	(11.4%)	(12.4%)	(11.6%)	(15.3%)
	CC-test	12	16	15	310	137	134	128	375
		(3.2%)	(4.2%)	(4.0%)	(82.0%)	(36.2%)	(35.4%)	(33.9%)	(99.2%)
$\alpha = 0.05$	*UC*-test	30	30	36	365	303	310	304	378
		(7.9%)	(7.9%)	(9.5%)	(96.6%)	(80.2%)	(82.0%)	(80.4%)	(100.0%)
	Ind-test	36	36	32	17	66	72	71	95
		(9.5%)	(9.5%)	(8.5%)	(4.5%)	(17.5%)	(19.0%)	(18.8%)	(25.1%)
	CC-test	38	39	47	349	183	201	189	376
		(10.1%)	(10.3%)	(12.4%)	(92.3%)	(48.4%)	(53.2%)	(50.0%)	(99.5%)
Specification (ii)									
		Model 1	Model 2	Model 3	Model 4	Model 1	Model 2	Model 3	Model 4
$\alpha = 0.01$	*UC*-test	12	17	28	361	134	139	126	372
		(3.2%)	(4.5%)	(7.4%)	(95.5%)	(35.4%)	(36.8%)	(33.3%)	(98.4%)
	Ind-test	7	12	10	5	70	70	73	272
		(1.9%)	(3.2%)	(2.6%)	(1.3%)	(18.5%)	(18.5%)	(19.3%)	(72.0%)
	CC-test	14	17	24	352	118	123	129	377
		(3.7%)	(4.5%)	(6.3%)	(93.1%)	(31.2%)	(32.5%)	(34.1%)	(99.7%)
$\alpha = 0.05$	*UC*-test	42	54	74	374	207	216	232	378
		(11.1%)	(14.3%)	(19.6%)	(98.9%)	(54.8%)	(57.1%)	(61.4%)	(100.0%)
	Ind-test	32	31	32	29	101	106	100	306
		(8.5%)	(8.2%)	(8.5%)	(7.7%)	(26.7%)	(28.0%)	(26.5%)	(81.0%)
	CC-test	44	63	75	368	165	173	180	377
		(11.6%)	(16.7%)	(19.8%)	(97.4%)	(43.7%)	(45.8%)	(47.6%)	(99.7%)
Specification (iii)									
		Model 1	Model 2	Model 3	Model 4	Model 1	Model 2	Model 3	Model 4
$\alpha = 0.01$	*UC*-test	293	311	324	378	304	317	328	378
		(77.5%)	(82.3%)	(85.7%)	(100.0%)	(80.4%)	(83.9%)	(86.8%)	(100.0%)
	Ind-test	3	5	4	3	16	15	17	234
		(0.8%)	(1.3%)	(1.1%)	(0.8%)	(4.2%)	(4.0%)	(4.5%)	(61.9%)
	CC-test	278	296	309	378	264	279	301	378
		(73.5%)	(78.3%)	(81.7%)	(100.0%)	(69.8%)	(73.8%)	(79.6%)	(100.0%)
$\alpha = 0.05$	*UC*-test	345	350	361	378	341	347	355	378
		(91.3%)	(92.6%)	(95.5%)	(100.0%)	(90.2%)	(91.8%)	(93.9%)	(100.0%)
	Ind-test	15	19	21	13	29	26	41	264
		(4.0%)	(5.0%)	(5.6%)	(3.4%)	(7.7%)	(6.9%)	(10.8%)	(69.8%)
	CC-test	325	338	350	378	312	327	338	378
		(86.0%)	(89.4%)	(92.6%)	(100.0%)	(82.5%)	(86.5%)	(89.4%)	(100.0%)
Specification (iv)									
		Model 1	Model 2	Model 3	Model 4	Model 1	Model 2	Model 3	Model 4
$\alpha = 0.01$	*UC*-test	18	10	27	253	253	232	231	374
		(4.8%)	(2.6%)	(7.1%)	(66.9%)	(66.9%)	(61.4%)	(61.1%)	(98.9%)
	Ind-test	12	10	14	8	39	45	49	244
		(3.2%)	(2.6%)	(3.7%)	(2.1%)	(10.3%)	(11.9%)	(13.0%)	(64.6%)
	CC-test	19	11	29	239	184	159	173	378
		(5.0%)	(2.9%)	(7.7%)	(63.2%)	(48.7%)	(42.1%)	(45.8%)	(100.0%)
$\alpha = 0.05$	*UC*-test	48	44	64	324	295	273	284	378
		(12.7%)	(11.6%)	(16.9%)	(85.7%)	(78.0%)	(72.2%)	(75.1%)	(100.0%)
	Ind-test	43	53	52	24	75	75	85	279
		(11.4%)	(14.0%)	(13.8%)	(6.3%)	(19.8%)	(19.8%)	(22.5%)	(73.8%)
	CC-test	71	71	85	315	226	208	224	378
		(18.8%)	(18.8%)	(22.5%)	(83.3%)	(59.8%)	(55.0%)	(59.3%)	(100.0%)

Note: The table shows the number and percentage of rejections of the unconditional coverage (UC), independence (Ind) and conditional coverage (CC) test for all 378 institutions at the 1% and the 5% significance level. Model 1 to Model 4 refer to the periodic model structures given in Table 4.

while the MF-GAS approximates long-memory via a mixed-frequency component framework, which combines short-memory GAS processes at different frequencies.

Following the Sklar (1959) theorem, the conditional bivariate Student's t distribution in (53) can be decomposed into univariate Student's t marginals coupled with the Student t copula with conditional correlation parameter ρ_τ (see, e.g., Nelsen, 2006), similar to the MF-GAS setting. According to the FIGAS model outlined above, we obtain $r_{i,\tau}|\mathcal{F}_{\tau-1} \sim t_1(V_{11,\tau}, \gamma_\ell)$, $r_{m,\tau}|\mathcal{F}_{\tau-1} \sim t_1(V_{22,\tau}, \gamma_\ell)$ and the Student t copula $C(u_{i,\tau}, u_{m,\tau}; \rho_\tau, \gamma_\ell|\mathcal{F}_{\tau-1})$ with $\rho_\tau = V_{12,\tau}/\sqrt{V_{11,\tau}V_{22,\tau}}$ and $(u_{i,\tau}, u_{m,\tau})$ being the probability integral transforms of $(r_{i,\tau}, r_{m,\tau})$ based on the marginal Student t cdf (compare Equation 30 and Equation 41 for details on the Student t copula). Note that the parameter matrix Ω_ℓ drives the unconditional covariance process of r^*_τ. Hence, we can directly apply models 1–4 of Table 4 for modeling the periodic structures of the FIGAS model. For this purpose, we separate intraday periodicity in volatilities (marginals) and correlations (copula) via a variance/correlation decomposition of Ω_ℓ, whose elements are then estimated individually for each intraday trading period ℓ, similar to the MF-GAS setting.

We consider four different specifications for out-of-sample forecasting of the (Δ)ECoVaR:

(i) The in-sample preferred V-MF-GAS-t- and C-MF-GAS-t_{κ_ℓ} copula models for the margins and the dependence structure.
(ii) Similar to Specification (i) but without the intraday volatility/dependence components z_τ and $\tilde{z}_\tau$ ($z_\tau = \tilde{z}_\tau = 0 \forall \tau$). The model structure then implies a GAS setting, where intraday variation is restricted to the periodicities.
(iii) Similar to Specification (i) but without the daily volatility/dependence components l_τ and $\tilde{l}_\tau$ ($l_t = \tilde{l}_t = 0 \forall t$). The model structure then implies a standard short-memory GAS setting without mixed frequency component.
(iv) The FIGAS model of Opschoor and Lucas (2019) detailed above.

For each of the specifications (i)-(iv) we consider the four seasonal structures of models 1–4 in Table 4.

Tables 5–7 provide the results on the out-of-sample (Δ)ECoVaR backtesting application. The tables report the absolute and relative number of rejections of the null of unconditional coverage (*UC*), independence of the hit-rate sequence (*Ind*), and conditional coverage (*CC*) at the 1% and the 5% significance level for all 378 asset-market combinations. For the discussion of the test results, we focus on the 5% level and the conditional coverage test, which aggregates both unconditional coverage and independence. Table 5 shows results for the complete out-of-sample period from 2008 to 2012. The overall best ECoVaR performance is achieved for the MF-GAS setting of Specification (i) and Model 1. Hence, a flexible dynamic modeling with periodicity in both, the volatilities and the dependence structure, appears important for ECoVaR forecasting. The FIGAS approach comes relatively close to the MF-GAS setting but is overall outperformed. The worst results are obtained for Specification (iii). We therefore conclude that long-term persistence as generated by the daily volatiltiy/dependence component appears to be crucial for ECoVaR forecasting. Turning to the ΔECoVaR, we observe a sharp increase in the rejection rates, which is explained by the joint testing for the ECoVaR and the benchmark ECoVaR, where the hit-rate tests for the latter involve thousands of data points, which easily drive the test statistics into significance. The best results are again obtained for the MF-GAS setting under Specification (i). From the discussion of Section 4.4.1, we would expect that the dependence pattern matters most for the ΔECoVaR. However, the overall best performance is achieved for Model 3, which neither contains periodicity in the correlation, nor the d.o.f. parameter. Nevertheless, Models 1 and 2 perform overall similar to Model 3 and only Model 4, which contains neither volatility nor dependence patterns, is clearly rejected by the data.

The results for the crisis period from 2008 to 2009 in Table 6 show a really good ECoVaR performance for the FIGAS model of Specification (iv) (Model 4) while the MF-GAS of Specification (i) is second best under Model 2. For the ΔECoVaR however the FIGAS is clearly outperformed with 100% rejection rates for all periodic model structures. The best ΔECoVaR performance is achieved for Specification (iii) under Model 1, that is, a standard GAS model without daily component and with periodicity in volatility and dependence—a result that may be explained by short-lived volatility and dependence shocks generated by single crisis events.

The best results for the calm period from 2010 to 2012 are obtained under the full periodic structure of Model 1, that is, periodicity for volatility and dependence (see Table 7). While the MF-GAS of Specification (i) performs best for the ECoVaR, the best ΔECoVaR forecasts are obtained under Specification (ii), which only contains a daily volatility component and no intraday dynamics.

Overall, we can conclude that the MF-GAS approach provides a solid out-of-sample (Δ)ECoVaR forecasting performance, where Models 1 and 2 with periodicity in both, the correlation and the volatility process, are typically the best performing models for the ECoVaR and the (Δ)ECoVaR measure. Except for the crisis period, the worst performance is typically obtained for Model 4,

which contains no periodicity at all. Hence, accounting for seasonal patterns in intraday volatilities appears to matter most for a solid (Δ)ECoVaR forecasting performance. Interestingly, while we would expect that the volatility (correlation) pattern is most important for the ECoVaR (ΔECoVaR), we cannot clearly identify separate effects of the respective periodicities in the hit-rate based backtesting application. In fact, accounting for periodicities in volatilities and correlations appears to be important for both measures.

Our hit-rate based backtesting experiment gives insights on the forecasting performance for a huge empirical data set. However, the analysis appears restrained due to the unavailability of the "true" (Δ)ECoVaR as a solid benchmark for assessing the forecasting performance. The results further represent an aggregation over various asset/market relations with different degrees of periodicity in the volatility and dependence structure. In order to obtain a deeper insight into the effects of the periodic structures in volatilities and dependencies on the (Δ)ECoVaR forecasts, we conduct an additional simulation-based forecasting experiment based on an artificial data set, which shows significant periodic effects in both, volatilities and dependence, and for which we observe the true simulated (Δ)ECoVaR measures. In particular, we use our most flexible model specification with V-MF-GAS-*t*- and C-MF-GAS-t_{κ_ℓ} processes for the margins and the copula (Specification (i)) in order to simulate an intraday return series of length equal to our empirical data ($T = 2265$, $S = 26$). For the parametrization, we choose our estimates for the PFG stock, which resembles data with significant intraday periodicity in all three cases: volatilities, correlations, and tail-dependence measures. The periodic patterns used for the simulation are depicted in Figure S4. We then conduct an out-of-sample forecasting experiment identical to the one outlined above but restricted to the V-MF-GAS-*t*- and C-MF-GAS-t_{κ_ℓ} processes of Specification (i). Because we observe the true ECoVaR and ΔECoVaR measures from the simulation, we are able to analyze the resulting forecasting errors directly.

Figure 8 uses boxplots in order to depict the distribution of the ECoVaR forecasting errors for the 26 intraday periods and the four periodic model structures of Table 4. The ECoVaR forecasts stay relatively unaffected by neglected intraday patterns in (non-)linear dependencies (Model 1 to Model 3) but are clearly influenced by the volatility pattern. The resulting biases for Model 4 reflect the *U* shaped seasonality in the volatilities: positive biases in the morning turn to negative biases after 10:15 a.m. until the bias finally vanishes in the afternoon. The forecasting results

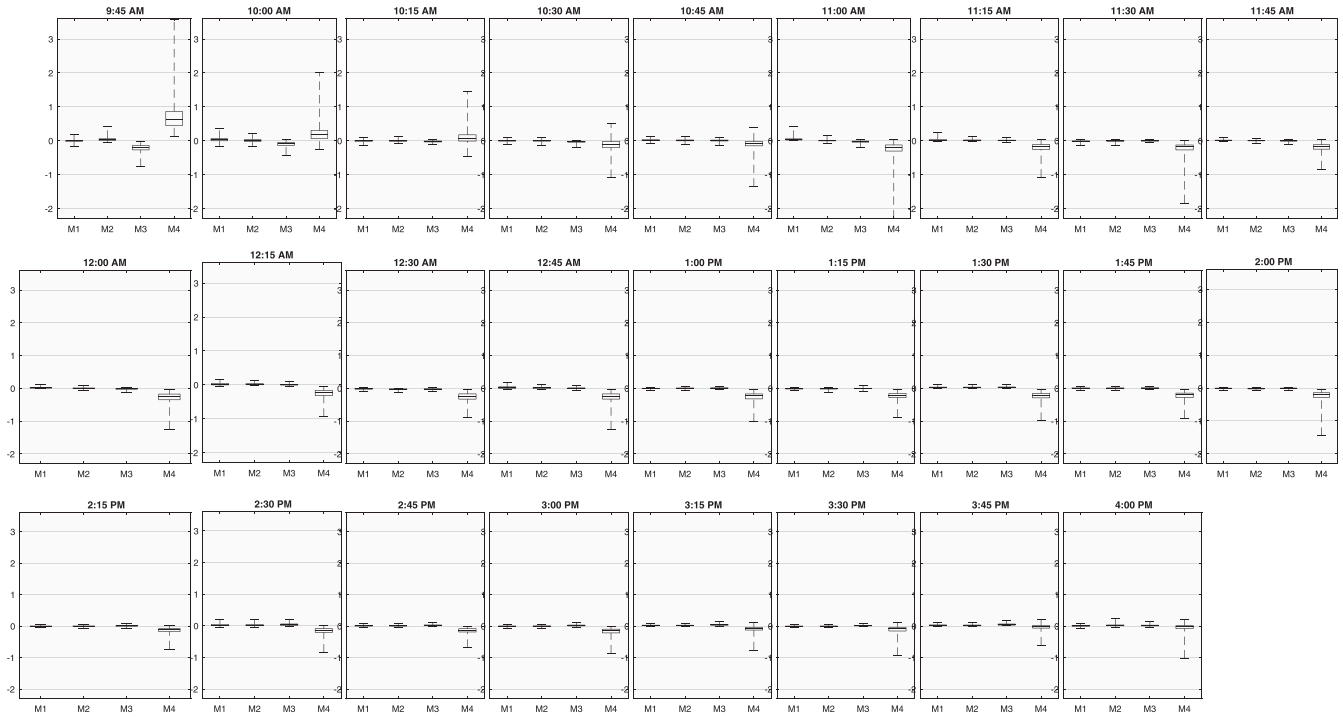

FIGURE 8 Distribution of the forecast errors of the out-of-sample ECoVaR forecasts for the simulated data set as detailed in Section 4.4.2 for each of the 26 intraday periods. The out-of-sample results are obtained by splitting the data set in the middle and reserving the second half of the time series as the forecasting window. The forecasting period then starts at July 2, 2008, and ends on December 31, 2012, covering a total of $1133 \times 26 = 29{,}458$ periods. Forecasts are generated iteratively with a rolling window scheme and the models are re-estimated at the end of each trading day. Hence, we obtain overall 1133 forecasts for each intraday period. M1 to M4 refer to the periodic model structures given in Table 4

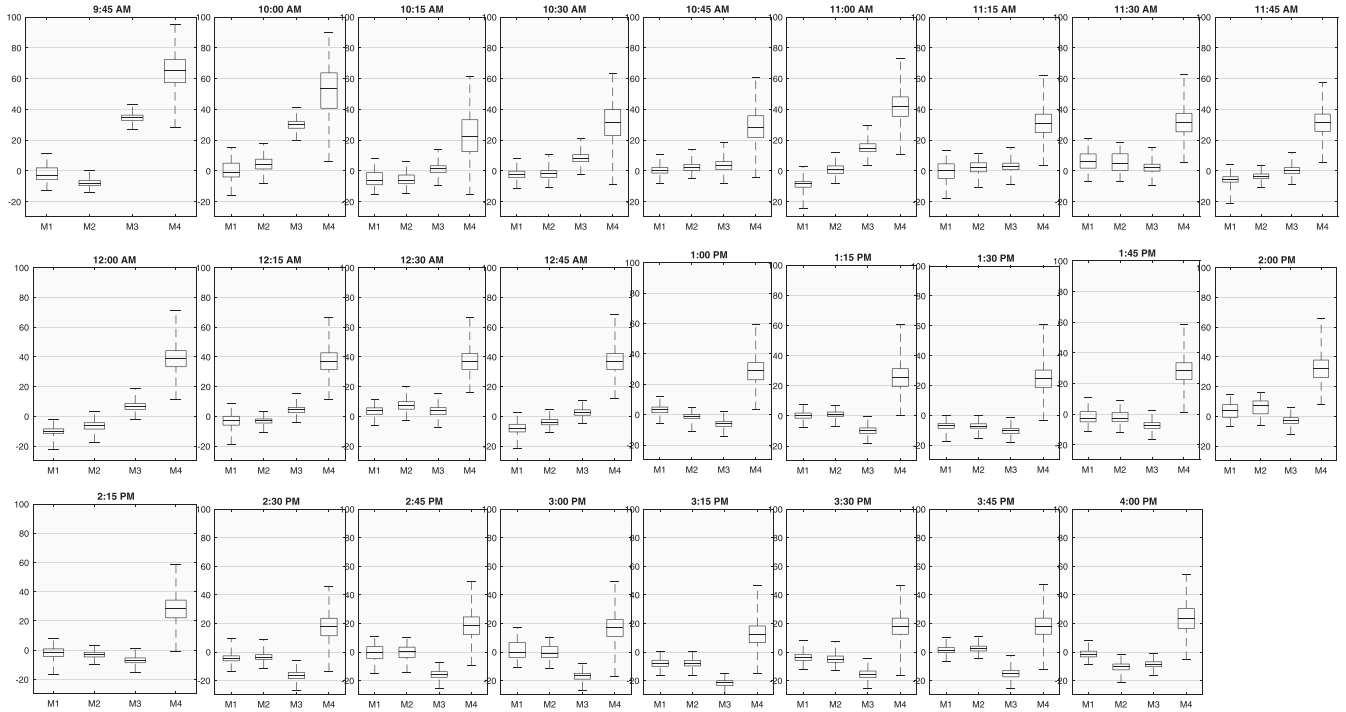

FIGURE 9 Distribution of the forecast errors of the out-of-sample ΔECoVaR forecasts for the simulated data set as detailed in Section 4.4.2 for each of the 26 intraday periods. The out-of-sample results are obtained by splitting the data set in the middle and reserving the second half of the time series as the forecasting window. The forecasting period then starts at July 2, 2008, and ends on December 31, 2012, covering a total of $1133 \times 26 = 29{,}458$ periods. Forecasts are generated iteratively with a rolling window scheme and the models are re-estimated at the end of each trading day. Hence, we obtain overall 1133 forecasts for each intraday period. M1 to M4 refer to the periodic model structures given in Table 4

for the ΔECoVaR are depicted in Figure 9. We observe a strong impact of neglecting volatility and correlation patterns in forecasting the ΔECoVaR measure. In particular, the biases under Model 3 show a negative trend over the trading day, which is explained by the neglected correlation trend in the data (see Figure S4). The impact of ignoring periodicity in the tail dependence appears negligible in most of the cases.

We can summarize that for the forecasting of the (Δ)ECoVaR measure it appears crucial to account for intraday periodicities. In particular for the ΔECoVaR it appears important to account for the positive trend of intraday asset-market correlations. Overall, the V-MF-GAS-*t*- and C-MF-GAS-t_κ models with constant d.o.f. for the copula part are a reasonable choice in practice. The models are easy to implement, fast to estimate and provide good out-of-sample results.

5 | CONCLUSION

We propose a copula-based periodic mixed frequency GAS framework in order to model and forecast the intraday ECoVaR for the bivariate relationship of an intraday asset return and the corresponding market return. The model combines latent short- and long-term components together with intraday seasonalities in order to account for the presence of long-memory type of dependence structures and periodicity in the marginal volatility and dependence dynamics. Both the short- and long-term components are assumed to follow individual GAS processes on the intraday and the daily frequency. The model is furthermore extended in order to account for intraday price jumps. We further investigate fat-tailed conditional return distributions for the univariate margins as well as several copula specifications in order to account for linear dependence and (a)symmetric tail dependence in the asset-market relationship.

We apply our framework to a large data set of intraday asset returns for 378 NYSE traded stocks. The data comprises 15-min intraday log returns for the period starting at January 2, 2004, and ending on December 31, 2012. The empirical application shows four major results. First, we find highly persistent intraday volatility and dependence processes together with significant intraday periodicities for volatilities, correlations, and nonlinear dependencies. Second, the mixed frequency approach based on a Student *t* copula with periodic or nonperiodic d.o.f. and Student's *t* margins provides a good model fit and represents a reasonable choice in practice in order to adequately estimate

the ECoVaR on an intraday basis. Third, while the intraday volatility pattern follows the typical inverted *U* shape, the correlations and tail dependencies show a positive trend over the trading day. Finally, the explicit modeling of the volatility and correlation pattern appears important for the out-of-sample forecasting of both the ECoVaR and the ΔECoVaR measure.

ACKNOWLEDGMENTS

The authors thank two anonymous referees for their helpful and very constructive comments. For helpful comments, we also thank seminar and conference participants at the 2019 CFE-CMStatistics conference. We are grateful to the Regional Computing Center at the University of Cologne for providing parts of the computational resources required. Open access funding enabled and organized by Projekt DEAL.

CONFLICT OF INTEREST

The authors declare that there is no conflict of interest.

FUNDING INFORMATION

This research did not receive any specific grant from funding agencies in the public, commercial, or not-for-profit sectors. Open Access funding enabled and organized by ProjektDEAL. WOA Institution: UNIVERSITAET ZU KOLN Blended DEAL: ProjektDEAL.

DATA AVAILABILITY STATEMENT

The data that support the findings of this study are available from www.quantquote.com. Restrictions apply to the availability of these data, which were used under license for this study. Data are available from www.quantquote.com with the permission of QuantQuote.

ORCID


Bastian Gribisch https://orcid.org/0000-0002-6289-1799

REFERENCES

Adrian, T., & Brunnermeier, M. K. (2016). CoVaR. *American Economic Review*, *106*(7), 1705–1741.

Andersen, T. G., & Bollerslev, T. (1997). Intraday periodicity and volatility persistence in financial markets. *Journal of Empirical Finance*, *4*, 115–158.

Andersen, T. G., & Bollerslev, T. (1998). DM-Dollar volatility: Intraday activity patterns, macroeconomic announcements, and longer-run dependencies. *Journal of Finance*, *53*, 219–265.

Bekierman, J., & Gribisch, B. (2017). A mixed frequency stochastic volatility model for intraday stock market returns. Working Paper.

Beltratti, A., & Morana, C. (1999). Computing value at risk with high frequency data. *Journal of Empirical Finance*, *5*, 431–455.

Bernardi, M., & Catania, L. (2016). Switching-GAS copula models with application to systemic risk. ArXiv working paper.

Bibinger, M., Hautsch, N., Malec, P., & Reiss, M. (2019). Estimating the spot covariation of asset prices—Statistical theory and empirical evidence. *Journal of Business and Economic Statistics*, *37*(3), 419–435.

Blasques, F., Koopman, S. J., & Lucas, A. (2015). Information theoretic optimality of observation driven time series models for continuous responses. *Biometrika*, *102*(2), 325–343.

Bollerslev, T. (1986). Generalized autoregressive conditional heteroskedasticity. *Journal of Econometrics*, *31*, 307–327.

Chen, C. Y., Härdle, W. K., & Okhrin, Y. (2019). Tail event driven networks of SIFIs. *Journal of Econometrics*, *208*(1), 282–298.

Christoffersen, P. (1998). Evaluating interval forecasts. *International Economic Review*, *39*, 841–862.

Colacito, R., Engle, R. F., & Ghysels, E. (2011). A component model for dynamic correlations. *Journal of Econometrics*, *164*(1), 45–59.

Corsi, F. (2009). A simple approximate long-memory model of realized volatility. *Journal of Financial Econometrics*, *7*, 174–196.

Creal, D., Koopman, S. J., & Lucas, A. (2011). A dynamic multivariate heavy-tailed model for time-varying volatilities and correlations. *Journal of Business and Economic Statistics*, *29*(4), 552–563.

Creal, D., Koopman, S. J., & Lucas, A. (2013). Generalized autoregressive score models with applications. *Journal of Applied Econometrics*, *28*, 777–795.

Deo, R., Hurvich, C., & Lu, Y. (2006). Forecasting realized volatility using a long-memory stochastic volatility model: Estimation, prediction and seasonal adjustment. *Journal of Econometrics*, *131*, 29–58.

Eckernkemper, T. (2018). Modeling systemic risk: Time-varying tail dependence when forecasting marginal expected shortfall. *Journal of Financial Econometrics*, *16*(1), 63–117.

Embrechts, P., Frey, R., & McNeil, A. J. (2015). *Quantitative Risk Management: Concepts, Techniques and Tools (Revised Edition)*. Princeton, New Jersey: Princeton University Press.

Engle, R. F. (1982). Autoregressive conditional heteroskedasticity with estimates of the variance of united kingdom inflation. *Econometrica*, *50*(4), 987–1007.

Engle, R. F., Ghysels, E., & Sohn, B. (2013). Stock market volatility and macroeconomic fundamentals. *Review of Economics and Statistics*, *95*(3), 776–797.

Engle, R. F., & Sokalska, M. E. (2012). Forecasting intraday volatility in the US equity market. Multiplicative component GARCH. *Journal of Financial Econometrics*, *10*(1), 4–83.

Ghysels, E., Santa-Clara, P., & Valkanov, R. (2006). Predicting volatility: Getting the most out of returns data sampled at different frequencies. *Journal of Econometrics*, *131*, 59–95.

Girardi, G., & Ergün, A. T. (2013). Systemic risk measurement: Multivariate GARCH estimation of CoVaR. *Journal of Banking and Finance*, *37*(8), 3169–3180.

Gorgi, P., Koopman, S. J., & Li, M. (2019). Forecasting economic time series using score-driven dynamic models with mixed-data sampling. *International Journal of Forecasting*, *35*(4), 1735–1747.

Gourieroux, C., & Jasiak, J. (1997). Local likelihood density estimation and Value-at-Risk. *Journal of Probability and Statistics*, *2010*, 1–26.

Granger, C. (1980). Long memory relationships and the aggregation of dynamic models. *Journal of Econometrics*, *14*, 227–238.

Grossmass, L., & Poon, S. (2015). Estimating dynamic copula dependence using intraday data. *Studies in Nonlinear Dynamics and Econometrics*, *19*(4), 501–529.

Hafner, C. M., & Manner, H. (2012). Dynamic stochastic copula models: estimation, inference and applications. *Journal of Applied Econometrics*, *27*(2), 269–295.

Harvey, A. C. (2013). *Dynamic models for volatility and heavy tails: With applications to financial and economic time series* (Vol. 52). Cambridge: Cambridge University Press.

Harvey, A. C., & Sucarrat, G. (2014). EGARCH models with fat tails, skewness and leverage. *Computational Statistics and Data Analysis*, *76*, 320–338.

Janus, P., Koopman, S. J., & Lucas, A. (2014). Long memory dynamics for multivariate dependence under heavy tails. *Journal of Empirical Finance*, *29*, 187–206.

Koopman, S. J., Lit, R., & Lucas, A. (2017). Intraday stochastic volatility in discrete price changes: The dynamic Skellam model. *Journal of the American Statistical Association*, *112*(520), 1490–1503.

Koopman, S. J., Lit, R., Lucas, A., & Opschoor, A. (2018). Dynamic discrete copula models for high-frequency stock price changes. *Journal of Applied Econometrics*, *33*(7), 966–985.

Koopman, S. J., Lucas, A., & Scharth, M. (2016). Predicting time-varying parameters with parameter-driven and observation-driven models. *Review of Economics and Statistics*, *98*(1), 97–110.

Kupiec, P. H. (1995). Techniques for verifying the accuracy of risk measurement models. *Journal of Derivatives*, *3*(2), 73–84.

LeBaron, B. (2001). Stochastic volatility as a simple generator of financial power laws and long memory. *Quantitative Finance*, *1*, 621–631.

Liesenfeld, R., & Richard, J.-F. (2003). Univariate and multivariate stochastic volatility models: Estimation and diagnostics. *Journal of Empirical Finance*, *10*(4), 505–531.

Liu, S., & Tse, Y. K. (2015). Intraday value-at-risk: An asymmetric autoregressive conditional duration approach. *Journal of Econometrics*, *189*(2), 437–446.

Maheu, J. M., & McCurdy, T. H. (2004). News arrival, jump dynamics, and volatility components for individual stock returns. *The Journal of Finance*, *59*(2), 755–793.

Mainik, G., & Schaanning, E. (2014). On dependence consistency of CoVaR and some other systemic risk measures. *Statistics and Risk Modeling*, *31*(1), 49–77.

Manner, H., & Reznikova, O. (2012). A survey on time-varying copulas: specification, simulations, and application. *Econometric Reviews*, *31*(6), 654–687.

Nelsen, R. B. (2006). *An introduction to copulas* (2nd ed.). New York: Springer. Science Business Media.

Opschoor, A., & Lucas, A. (2019). Fractional integration and fat tails for realized covariance kernels. *Journal of Financial Econometrics*, *17*(1), 66–90.

Payne, R. (1996). Announcement effects and seasonality in the intra-day foreign exchange market. Financial Markets Group Discussion Paper, no. 238. LSE.

Reboredo, J. C., & Ugolini, A. (2015). Systemic risk in European Sovereign debt markets: A CoVaR-copula approach. *Journal of International Money and Finance*, *51*, 214–244.

Rossi, E., & Fantazzini, D. (2015). Long memory and periodicity in intraday volatility. *Journal of Financial Econometrics*, *13*(4), 922–961.

Sklar, A. (1959). Fonctions de Répartition à n dimensions et Leurs Marges. *Publications de l'Institut Statistique de l'Université de Paris*, *8*, 229–231.

Stroud, J. R., & Johannes, M. S. (2014). Bayesian modeling and forecasting of 24-hour high-frequency volatility. *Journal of the American Statistical Association*, *109*(508), 1368–1384.

Sun, W., Rachev, S. Z., & Fabozzi, F. J. (2008). Long-range dependence, fractal processes, and intra-daily data. In Bernus, P., Baewics, J., Schmidt, G., Shaw, M., Seese, D., Weinhardt, C., & Schlottmann, F. (Eds.), *Handbook on Information Technology in Finance* (pp. 543–585). Berlin Heidelberg: Springer.

AUTHOR BIOGRAPHIES

Tobias Eckernkemper studied Business Administration and Economics at the University of Cologne, Germany, from 2007 to 2013. From 2014 to 2019, he was a PhD student at the Institute of Econometrics and Statistics at the University of Cologne, where he received his PhD in February 2019.

Bastian Gribisch studied Economics at the University of Kiel, Germany, from 2004 to 2008. He joined the Department of Statistics and Econometrics at the University of Kiel as a PhD student in September 2008 and received his PhD in February 2013. From 2013 to 2015, he was working as a Postdoc at the University of Cologne, Germany, and since August 2015, he is working as an Assistant Professor ("Akademischer Rat") of Econometrics at the University of Cologne.

SUPPORTING INFORMATION

Additional supporting information may be found online in the Supporting Information section at the end of the article.

How to cite this article: Eckernkemper T, Gribisch B. Intraday conditional value at risk: A periodic mixed-frequency generalized autoregressive score approach. *Journal of Forecasting*. 2021;40:883–910. https://doi.org/10.1002/for.2744

APPENDIX A

A.1 | Gaussian Copula

For the bivariate Gaussian copula with time-varying correlation parameter $\rho_\tau \in (-1, 1)$, the Fisher information for

the C-MF-GAS model obtains as

$$E[(\nabla_\tau^{(\tilde{z})})^2|\mathcal{F}_{\tau-1}] = \frac{\dot{\rho}_\tau^2(1+\rho_\tau^2)}{(1-\rho_\tau^2)^2}, \tag{A1}$$

$$E[(\nabla_t^{(\tilde{l})})^2|\mathcal{F}_{t-1}] = \sum_{j=1}^{S} E[(\nabla_{(t-1)\cdot q+j}^{(\tilde{z})})^2|\mathcal{F}_{\tau-1}]. \tag{A2}$$

A.2 | Student's *t* Copula

For the bivariate Student's *t* copula with time-varying correlation parameter $\rho_\tau \in (-1,1)$ and time-constant degrees of freedom parameter $\kappa > 4$, the Fisher information for the C-MF-GAS model obtains as

$$\begin{aligned}
\frac{\partial c_1(u_{1,\tau},u_{2,\tau})}{\partial \theta_{1\tau}} =& \left\{ \frac{(\theta_{1\tau}+1)}{(u_{1\tau}u_{2\tau})^{\theta_{1\tau}+1}} \left[\frac{\left(\frac{\log(u_{1\tau})}{{u_{1\tau}}^{\theta_{1\tau}}} + \frac{\log(u_{2\tau})}{{u_{2\tau}}^{\theta_{1\tau}}}\right)\left(\frac{1}{\theta_{1\tau}}+2\right)}{\left({u_{1\tau}}^{-\theta_{1\tau}} + {u_{2\tau}}^{-\theta_{1\tau}} - 1\right)^{\frac{1}{\theta_{1\tau}}+3}} \right.\right. \\
&\left.\left. + \frac{\log\left({u_{1\tau}}^{-\theta_{1\tau}} + {u_{2\tau}}^{-\theta_{1\tau}} - 1\right)}{\theta_{1\tau}^2\left({u_{1\tau}}^{-\theta_{1\tau}} + {u_{2\tau}}^{-\theta_{1\tau}} - 1\right)^{\frac{1}{\theta_{1\tau}}+2}} \right] \right\} \\
&+ \frac{\left(1 - \log\left(u_{1\tau}u_{2\tau}\right)(\theta_{1\tau}+1)\right)}{(u_{1\tau}u_{2\tau})^{\theta_{1\tau}+1}\left({u_{1\tau}}^{-\theta_{1\tau}} + {u_{2\tau}}^{-\theta_{1\tau}} - 1\right)^{\frac{1}{\theta_{1\tau}}+2}}
\end{aligned} \tag{A5}$$

$$\begin{aligned}
\frac{\partial c_2(u_{1,\tau},u_{2,\tau})}{\partial \theta_{2\tau}} =& \left\{ \frac{(\theta_{2\tau}+1)}{((1-u_{1\tau})(1-u_{2\tau}))^{\theta_{2\tau}+1}} \left[\frac{\left(\frac{\log((1-u_{1\tau}))}{(1-u_{1\tau})^{\theta_{2\tau}}} + \frac{\log((1-u_{2\tau}))}{(1-u_{2\tau})^{\theta_{2\tau}}}\right)\left(\frac{1}{\theta_{2\tau}}+2\right)}{\left((1-u_{1\tau})^{-\theta_{2\tau}} + (1-u_{2\tau})^{-\theta_{2\tau}} - 1\right)^{\frac{1}{\theta_{2\tau}}+3}} \right.\right. \\
&\left.\left. + \frac{\log\left((1-u_{1\tau})^{-\theta_{2\tau}} + (1-u_{2\tau})^{-\theta_{2\tau}} - 1\right)}{\theta_{2\tau}^2\left((1-u_{1\tau})^{-\theta_{2\tau}} + (1-u_{2\tau})^{-\theta_{2\tau}} - 1\right)^{\frac{1}{\theta_{2\tau}}+2}} \right] \right\} \\
&+ \frac{\left(1 - \log\left((1-u_{1\tau})(1-u_{2\tau})\right)(\theta_{2\tau}+1)\right)}{((1-u_{1\tau})(1-u_{2\tau}))^{\theta_{2\tau}+1}\left((1-u_{1\tau})^{-\theta_{2\tau}} + (1-u_{2\tau})^{-\theta_{2\tau}} - 1\right)^{\frac{1}{\theta_{2\tau}}+2}}.
\end{aligned} \tag{A6}$$

$$\begin{aligned}
E[(\nabla_\tau^{(\tilde{z})})^2|\mathcal{F}_{\tau-1}] =& \left(1-\rho_\tau^2\right)^{-2} \\
&\times \left(1 + \rho_\tau^2 - \frac{2\rho_\tau^2}{\kappa+2}\right)\left(\frac{\kappa+2}{\kappa+4}\right)\dot{\rho}_\tau^2,
\end{aligned} \tag{A3}$$

$$E[(\nabla_t^{(\tilde{l})})^2|\mathcal{F}_{t-1}] = \sum_{j=1}^{S} E[(\nabla_{(t-1)\cdot q+j}^{(\tilde{z})})^2|\mathcal{F}_{\tau-1}]. \tag{A4}$$

A.3 | CrC Copula

For the CrC copula with time-varying copula parameters $\theta_{1\tau} > 0$, $\theta_{2\tau} > 0$ and time-constant mixture weight w the derivatives needed for the scores in Equations (49) and (50) obtain as

Because it appears complex to derive the Fisher information for the C-MF-GAS model under the CrC copula, we set the corresponding scaling coefficients to one ($s_\tau^{(\tilde{z})} = s_\tau^{(\tilde{l})} = 1$).